THE ASTROPHYSICAL JOURNAL, 460:869–894, 1996 April 1

SILICON BURNING. I. NEUTRONIZATION AND THE PHYSICS OF QUASI-EQUILIBRIUM

W. RAPHAEL HIX
Harvard-Smithsonian Center for Astrophysics, 60 Garden Street, Cambridge, MA 02138; raph@cfa.harvard.edu
AND
FRIEDRICH-KARL THIELEMANN
Institut für theoretische Physik, Universität Basel, Klingelbergstrasse 82, CH-4056 Basel, Switzerland; fkt@quasar.physik.unibas.ch
Received 1995 February 3; accepted 1995 October 4

ABSTRACT

As the ultimate stage of stellar nucleosynthesis, and the source of the iron peak nuclei, silicon burning is important to our understanding of the evolution of massive stars and supernovae. Our reexamination of silicon burning, using results gleaned from simulation work done with a large nuclear network (299 nuclei and more than 3000 reactions) and from independent calculations of equilibrium abundance distributions, offers new insights into the quasi-equilibrium mechanism and the approach to nuclear statistical equilibrium. We find that the degree to which the matter has been neutronized is of great importance, not only to the final products but also to the rate of energy generation and the membership of the quasi-equilibrium groups. A small increase in the global neutronization results in much larger free-neutron fluences, increasing the abundances of more neutron-rich nuclei. As a result, incomplete silicon burning results in neutron richness among the isotopes of the iron peak much larger than the global neutronization would indicate. Finally, we briefly discuss the limitations and pitfalls of models for silicon burning currently employed within hydrodynamic models. In a forthcoming paper we will present a new approximation to the full nuclear network which preserves the most important features of the large nuclear network calculations at a significant improvement in computational speed. Such improved methods are ideally suited for hydrodynamic calculations which involve the production of iron peak nuclei, where the larger network calculation proves unmanageable.

Subject headings: nuclear reactions, nucleosynthesis, abundances

1. INTRODUCTION

With the exhaustion of hydrogen in the core of a massive star, an inexorable contraction begins, heating and compressing the core, delayed for a time as each succeeding nuclear fuel ignites and is transformed. Beginning with the helium ash of hydrogen burning, most of these burning stages consist of fusion reactions among the nuclei of the ash. The first exception is neon burning. Following carbon burning, which leaves behind ash composed of O, Ne, and Mg, the temperature and density continue to rise. Before the temperature is adequate to allow fusion reactions among O nuclei to overcome the Coulomb repulsion, the photon field becomes sufficiently energetic to photodissociate Ne. In general, a photodisintegration channel becomes important when the Q-value of the reaction, that is, the energy difference between fuel and products, is smaller than approximately $30k_B T$. For such temperatures, the high-energy tail of the Planck distribution provides enough photons of sufficient energy that the photodisintegration reaction represents a comparable flow. With a Q-value of 4.7 MeV, $^{20}\mathrm{Ne}(\gamma, \alpha)^{16}\mathrm{O}$ becomes important for temperatures above 1.5×10^9 K. Thus the next stage is neon burning, typified by the photodisintegration of neon and the subsequent capture of the ejected α-particles by the remaining heavy ions. With the exhaustion of this energy source, the collapse continues until the O nuclei are sufficiently energetic to fuse. Once more, nuclear burning offers a respite until the oxygen fuel is exhausted and the collapse continues, further raising the temperature and density. With typical Q-values for reactions among stable nuclei above silicon being 8–12 MeV, photodisintegration begins to play an important role for all nuclei once the temperature exceeds 3×10^9 K. Nuclei with the smallest binding energies are destroyed in favor of their more tightly bound neighbors. Very quickly this leaves the core composed of silicon isotopes and their α nuclei neighbors, S, Ar, and Ca, the most bound of the light nuclei. Continued contraction further increases temperatures, favoring even more tightly bound nuclei, the iron peak. What follows is a complex series of photodissociation and capture reactions, converting silicon into iron peak elements. Unlike previous burning stages, where a few reactions (either heavy-ion reactions among the principal constituents or conversion among neighbors initiated by photodisintegration) dominated, here the fuel nuclei are linked to the product nuclei by a multitude of reaction chains and cycles. Since these chains of reactions wind their way through many nuclei intermediate between silicon and the iron peak nuclei, it is necessary to keep track of many more nuclei than was the case for prior burning stages. With four potential particles in the incoming channel, p, n, α, or γ, and these same four choices for the outgoing channels, discounting elastic scattering reactions, there are, in principle, at least 12 reactions per nucleus. Thus silicon burning is a complicated web of reactions, making it necessary to keep track of the abundances of a large number of nuclei. This is a major contribution to the complexity of silicon burning.

Silicon burning is further complicated by the closeness to equilibrium of many of these pairs of photodissociations and capture reactions. Net fluxes are often orders of magnitude smaller than either the forward or reverse reaction rates would indicate. Considering that the end state of silicon burning is an equilibrium, nuclear statistical equilibrium (NSE), it is hardly surprising that equilibria among

nuclei arise during silicon burning. From a purely numerical point of view, the net reaction flux being the difference of two large numbers raises the potential danger of round-off errors. However, equilibria are attractive for the simplification they provide. As we will see, equilibria are the key to understanding silicon burning and simplifying our modeling thereof.

The work of Bodansky, Clayton, & Fowler (1968, hereafter BCF) examined the process by which this equilibrium distribution is formed. Burbidge et al. (1957, hereafter B^2FH) had postulated that the intermediate nuclei, principally the α-particle nuclei from ^{24}Mg to ^{40}Ca, were formed by the α-process, a series of α-particle captures, which was separate from the e-process which formed the iron peak. Taking their cue from Hayashi et al. (1959) and the nuclear network calculations of Truran, Cameron, & Gilbert (1965), BCF showed that the intermediate nuclei are formed via a partial equilibrium in which groups of nuclei exist which are internally in equilibrium under the exchange of photons, protons, neutrons, and α-particles, i.e., in equilibrium with respect to strong and electro-magnetic reactions. These quasi-equilibrium (QSE) groups remain out of equilibrium with respect to other groups until the final complete equilibrium is achieved. BCF concluded that the abundances of the intermediate nuclei could be explained by a single QSE group which reached from ^{28}Si through the iron peak, but which failed to reach complete equilibrium, or to completely exhaust silicon. Thus the α- and e-processes of B^2FH were unified, coinciding with silicon burning, which had been determined to be a fundamental late stage of nuclear burning in massive stars. Further, BCF examined the influence of weak reactions on silicon burning and concluded that, while these reactions could have important effects on the abundance distribution, the ratio of the total number of protons to the total number of neutrons did not vary far from unity. In contrast to Fowler & Hoyle (1964), BCF concluded that the dominance of ^{56}Fe was due to the production of ^{56}Ni, which subsequently decayed to ^{56}Co and then to ^{56}Fe. This scenario agrees well with observations of supernovae. The lack of an equilibrium among weak reactions requires the monitoring of an additional degree of freedom which affects the equilibrium solution, the degree to which the material is neutronized. In the literature this is parameterized in two ways, as Y_e, the electron (molar) abundance, or as η, the neutron excess parameter:

$$Y_e = \sum_i Z_i Y_i = \sum_i \left(\frac{Z_i}{A_i}\right) X_i , \tag{1a}$$

$$\eta = \sum_i (N_i - Z_i) Y_i = \sum_i \left(\frac{N_i - Z_i}{A_i}\right) X_i$$

$$= \sum_i \left(\frac{A_i - 2Z_i}{A_i}\right) X_i , \tag{1b}$$

$$\eta = 1 - 2Y_e , \tag{1c}$$

where Z_i, N_i, A_i, X_i, and Y_i are respectively the atomic number, neutron number, mass number, mass fraction, and abundance of nucleus i. Physically, Y_e is the ratio of protons to nucleons (identical to the ratio of electrons to nucleons, hence the subscript e) or the total proton fraction, and η is the fraction of excess neutrons per nucleon. BCF showed that the abundances which result from silicon burning are strongly dependent on the degree of neutronization, a view reinforced by Hartmann, Woosley, & El Eid (1985). In this paper we will show that not only the nuclear products but the entire mechanism is strongly affected by the degree of neutronization.

Woosley, Arnett, & Clayton (1973, hereafter WAC), in the context of parameterized explosive silicon burning, showed that rather than a single QSE group between silicon and the iron peak, there are initially two groups, roughly divided by $A \simeq 45$. WAC further demonstrated that considering only the reactions which link the groups yields a good approximation of the time necessary for the two groups to merge and form a single QSE group. Indeed, WAC contended that this linkage was dominated by a single reaction, ^{45}Sc(p, γ)^{46}Ti, with perhaps a quarter of the flow going through less important reactions like ^{42}Ca(α, γ)^{46}Ti and ^{45}Ti(n, γ)^{46}Ti. In later sections we will show that for material which has been more highly neutronized, these two QSE groups form further from mutual equilibrium and that this division persists for a much longer time. In addition, there is some ambiguity in defining the boundary between the QSE groups and the most important reactions linking the groups as Y_e is varied. As we will also show, the dependence of the behavior of the QSE groups on the degree of neutronization has important consequences for the energy generation and other physical manifestations of silicon burning, in addition to determining the nuclear products.

Thielemann & Arnett (1985, hereafter TA), examined silicon burning in the context of hydrostatic models of massive stars and noticed behavior largely in keeping with that described by WAC for the explosive case. For conditions characteristic of the cores of more massive stars, high temperature, low density, and consequently larger Y_e, TA found that the bottleneck between the QSE groups, coinciding roughly with $Z = 21$, was bridged on the proton-rich side of stability. However, for conditions more characteristic of lower mass stars, lower temperature, higher density, and smaller Y_e, the bridge was found to be proton capture on neutron-rich isotopes of Ca. This more complex behavior differed with the assertions of WAC and of Weaver, Woosley, & Fuller (1985) that the single reaction ^{45}Sc(p, γ)^{46}Ti is responsible for the lion's share of the flow between the QSE groups. As we will show in later sections, our efforts allow us to explain the differences between the results of TA and WAC.

2. NUCLEAR REACTION NETWORK CALCULATION

Silicon burning in the cores of massive stars takes place under a range of temperatures and densities and with a range of electron fractions. We have examined silicon burning in a cube of this parameter space with temperatures in the range (3.5–5) $\times$ 10^9 K, densities between 10^7 and 10^{10} g cm^{-3}, and Y_e between 0.498 and 0.46, using a nuclear network of 299 nuclei, shown in Table 1. This region of parameter space roughly spans the region that previous investigations of nucleosynthesis in massive stars (Thielemann & Arnett 1985; Nomoto & Hashimoto 1988) have exhibited during core silicon burning. Further, the lower density portions of this parameter space overlap, to a large extent, the parameter space that prior investigations (WAC; Woosley, Pinto, & Weaver 1988; Thielemann, Hashimoto, & Nomoto 1990; Aufderheide, Baron, & Thielemann 1991) have determined appropriate for explosive

TABLE 1

NUCLEAR SET INCLUDED IN CALCULATIONS

Element	A_{min}	A_{max}	Element	A_{min}	A_{max}
n.....	1	1	Cl	31	40
H.....	1	3	Ar	33	44
He[a].....	3	6	K.....	35	46
Li	6	8	Ca	37	49
Be[a]	7	11	Sc	40	50
B[a]	8	12	Ti	42	52
C	10	15	V	44	54
N.....	12	17	Cr	46	56
O.....	14	20	Mn.....	48	58
F	17	21	Fe.....	50	62
Ne	18	25	Co	52	63
Na	20	26	Ni.....	54	67
Mg.....	21	28	Cu	57	69
Al	23	30	Zn	59	72
Si.....	25	33	Ga	61	74
P	27	35	Ge	63	78
S	29	38			

[a] Excepting ^{5}He, ^{8}Be, and ^{9}B.

silicon burning. We have included the effects of Coulomb screening on the equilibria for this same region of parameter space, as discussed in Hix et al. (1996). The results of nuclear network calculations for this region of parameter space and the comparison of these network calculations with equilibrium calculations are discussed in the present paper. In a subsequent paper (Hix & Thielemann 1996, hereafter Paper II), we will discuss the applicability of quasi-equilibrium to explosive burning. The final goal is an improvement to the network, using what we have learned about QSE, which speeds the calculation of the energy generation and nuclear abundance changes due to silicon burning, preserving much of the accuracy of the network calculation while greatly reducing the computational overhead.

For our study of silicon burning, we consider 299 nuclei, listed with mass numbers in Table 1, linked by more than 3000 reactions. This nuclear set stretches from protons and neutrons to germanium. With 11 or more isotopes per element around and above iron and seven or more in the region around silicon, this nuclear set is more complete than that used in earlier work discussed in § 1. This improvement is most important for material which has undergone significant prior electron capture and hence has a Y_e significantly less than 0.498. Rather than complicate our task by including hydrodynamics, we have instead done a parameter study of silicon burning as a function of three variables, temperature, density, and Y_e. In the course of a hydrodynamic model calculation, the star's core would wind its way through our cube of parameter space. In particular, electron capture will cause Y_e to decrease with time. However, the timescales for changes in Y_e via weak reactions, even at densities sufficient for significant electron capture, are much longer than the timescales for the strong and electromagnetic reactions. Thus it is possible to treat them separately. Therefore, we have neglected weak reactions, allowing us to treat Y_e as a constant parameter rather than merely considering the Y_e at one point in time. The reaction rates for light nuclei are based on experimental information from Caughlan & Fowler (1988), Bao & Käppeler (1987), Wiescher et al. (1989), and also from Wagoner (1969) and Wagoner, Fowler, & Hoyle (1967) if otherwise unavailable. For intermediate and heavy nuclei, where higher level densities permit application of statistical model calculations, rates by Thielemann, Arnould, & Truran (1987) are used (see also Cowan, Thielemann, & Truran 1991). We utilized a reaction network at constant temperature, density, and Y_e, with Y_e set by an initial distribution of silicon isotopes. There are of course several such distributions with the same Y_e but, with the exception of a brief initial adjustment phase which does not enter into our analysis, such variations of the initial distribution showed the same results. The basics of a nuclear reaction network are summarized in Woosley (1986) or Thielemann, Nomoto, & Hashimoto (1994). It is particularly important to note that the weak and intermediate screening prescriptions of Graboske et al. (1973) were used, as well as the strong screening prescription of Itoh, Kuwashima, & Munakatu (1990). Transition among these prescriptions is performed by utilizing the smallest predicted screening enhancement.

3. THE PHYSICS OF QUASI-EQUILIBRIUM

Previous authors, notably BCF and WAC, have shown that QSE is a most important aid to understanding the process of silicon burning. This is fortunate, as it is much easier to follow the evolution of equilibrium groups rather than become lost in the welter of individual abundances and reactions. Since ^{28}Si is the principal fuel, we will begin our discussion of QSE here. If we take ^{28}Si to be the focus of our QSE group, then the abundance of a nucleus ^AZ which is in equilibrium with ^{28}Si with respect to the exchange of free nucleons, α-particles, and photons is

$$Y_{\rm QSE}(^AZ) = \left[\frac{C(^AZ)}{C(^{28}{\rm Si})}\right] Y(^{28}{\rm Si})\, Y_n^{N-14} Y_p^{Z-14}\,, \qquad (2)$$

where Y_n, Y_p, and $Y(^{28}$Si) are the abundances of free neutrons, free protons, and ^{28}Si, and we have defined

$$C(^AZ) = \frac{G(^AZ)}{2^A}\left(\frac{\rho N_{\rm A}}{\theta}\right)^{A-1} A^{3/2} \exp\left[\frac{B(^AZ)}{k_{\rm B}T}\right] \qquad (3)$$

for later convenience. $G(^AZ)$ and $B(^AZ)$ are the partition function and binding energy of the nucleus ^AZ, $N_{\rm A}$ is Avogadro's number, $k_{\rm B}$ is Boltzmann's constant, and ρ and T are the density and temperature of the plasma. Thus, the abundance of a nucleus in QSE with ^{28}Si is a function of three other abundances, those of free protons, free neutrons, and ^{28}Si, and the thermodynamic conditions and properties of the nucleus, subsumed here within $C(^AZ)$. It is the evolution of these three abundances which determine the behavior of the entire QSE group. We reserve $Y_{\rm QSE}(^AZ)$ to represent the abundance of a nuclear species in QSE with ^{28}Si. Equation (2) is identical to the expressions for QSE introduced by BCF and WAC, provided the α-particles, protons, and neutrons are internally in equilibrium. We find this provision to be justified by the time QSE is established.

This derivation ignores screening, an omission which Hix et al. (1996) found can be significant for equilibria under the conditions we are discussing. A rederivation including the screening corrections to the reaction balance produces

$$Y_{\rm QSE}(^AZ) = \left[\frac{C(^AZ)}{C(^{28}{\rm Si})}\right] \times Y(^{28}{\rm Si})\, Y_n^{N-14}\, Y_p^{Z-14} \prod_{Z'=14}^{Z-1} \left\{\frac{\exp\,[H_{p,\gamma}(Z')]}{\exp\,[H_{\gamma,p}(Z')]}\right\}, \qquad (4)$$

where $\exp[H_{ij}(Z')]$ is the screening correction for the reaction ${}^{A'}Z'(i,j){}^{A''}Z''$, and we utilize the convention that, for indices less than the bottom index ($Z < 14$), the product is instead a division. The form of this equation is perhaps not surprising. We can rewrite equation (4) in the suggestive form

$$Y_{\rm QSE}({}^{A}Z) = \frac{N_1}{D_1}\, Y({}^{28}{\rm Si})\,, \tag{5}$$

where

$$N_1 = C({}^{A}Z) Y_n^N Y_p^Z \prod_{Z'=1}^{Z-1} \left\{ \frac{\exp[H_{p,\gamma}(Z')]}{\exp[H_{\gamma,p}(Z')]} \right\}$$

and

$$D_1 = C({}^{28}{\rm Si}) Y_n^{14} Y_p^{14} \prod_{Z'=1}^{13} \left\{ \frac{\exp[H_{p,\gamma}(Z')]}{\exp[H_{\gamma,p}(Z')]} \right\}.$$

As $Y({}^{28}{\rm Si})$, Y_p, and Y_n approach their NSE values,

$$Y({}^{28}{\rm Si}) \Rightarrow Y_{\rm NSE}({}^{28}{\rm Si}) \equiv C({}^{28}{\rm Si}) Y_n^{14} Y_p^{14} \prod_{Z'=1}^{13} \left\{ \frac{\exp[H_{p,\gamma}(Z')]}{\exp[H_{\gamma,p}(Z')]} \right\}, \tag{6}$$

forcing

$$Y_{\rm QSE}({}^{A}Z) \Rightarrow C({}^{A}Z) Y_n^N Y_p^Z \prod_{Z'=1}^{Z-1} \left\{ \frac{\exp[H_{p,\gamma}(Z')]}{\exp[H_{\gamma,p}(Z')]} \right\} \equiv Y_{\rm NSE}({}^{A}Z)\,. \tag{7}$$

Thus the QSE group blends simply into the NSE distribution as ^{28}Si and the free nucleons approach equilibrium.

To compare the network results to quasi-equilibrium, we define

$$r_{\rm QSE}({}^{A}Z) \equiv \log\left[\frac{Y_{\rm QSE}({}^{A}Z)}{Y({}^{A}Z)} \right], \tag{8}$$

with $Y({}^{A}Z)$ being the network abundance; $Y_{\rm QSE}({}^{A}Z)$ is calculated from the network abundances of free nucleons and ^{28}Si. For comparison, this definition is compatible with $r_{\rm qe}$ as defined by WAC. Figures 1*a*–1*g* show the results of this comparison for varying degrees of silicon exhaustion, at different temperatures, densities, and values of Y_e. Before we consider the results, it is instructive to determine the signature that multiple QSE groups leave on $r_{\rm QSE}({}^{A}Z)$.

If a nucleus ${}^{A}Z$ is in QSE with, for example, ^{56}Ni, then there is an expression analogous to equation (4) or equation (5) for this abundance. Taking equation (5) as the template, we can define a second QSE abundance with respect to ^{56}Ni,

$$Y_{\rm QSE2}({}^{A}Z) \equiv \frac{N_2}{D_2}\, Y^{56}({\rm Ni})\,, \tag{9}$$

where

$$N_2 = C({}^{A}Z) Y_n^N Y_p^Z \prod_{Z'=1}^{Z-1} \left\{ \frac{\exp[H_{p,\gamma}(Z')]}{\exp[H_{\gamma,p}(Z')]} \right\}$$

and

$$D_2 = C({}^{56}{\rm Ni}) Y_n^{28} Y_p^{28} \prod_{Z'=1}^{27} \left\{ \frac{\exp[H_{p,\gamma}(Z')]}{\exp[H_{\gamma,p}(Z')]} \right\}.$$

For species which are part of this second QSE group, i.e., $Y({}^{A}Z) = Y_{\rm QSE2}({}^{A}Z)$, using equations (9) and (5) we can evaluate

$$\frac{Y_{\rm QSE}({}^{A}Z)}{Y({}^{A}Z)} = \frac{Y_{\rm QSE}({}^{A}Z)}{Y_{\rm QSE2}({}^{A}Z)} = \frac{(N_1/D_1) Y({}^{28}{\rm Si})}{(N_2/D_2) Y({}^{56}{\rm Ni})}\,. \tag{10}$$

Since the numerators of these fractions, N_1 and N_2, are identical, cancellation leaves

$$\frac{Y_{\rm QSE}({}^{A}Z)}{Y({}^{A}Z)} = \left[C({}^{56}{\rm Ni}) Y_n^{28} Y_p^{28} \prod_{Z'=1}^{27} \left\{ \frac{\exp[H_{p,\gamma}(Z')]}{\exp[H_{\gamma,p}(Z')]} \right\} \Big/ C({}^{28}{\rm Si}) Y_n^{14} Y_p^{14} \prod_{Z'=1}^{13} \left\{ \frac{\exp[H_{p,\gamma}(Z')]}{\exp[H_{\gamma,p}(Z')]} \right\} \right] \frac{Y({}^{28}{\rm Si})}{Y({}^{56}{\rm Ni})} = \frac{Y_{\rm QSE}({}^{56}{\rm Ni})}{Y({}^{56}{\rm Ni})} \tag{11}$$

Thus every member of a QSE group has the same value of $r_{\rm QSE}({}^{A}Z)$. For the silicon group, $r_{\rm QSE}({}^{A}Z) = 0$, but other groups will also be apparent but offset from zero. Although free nucleons do not come into equilibrium with ^{28}Si until NSE is established, it is also instructive to examine $r_{\rm QSE}(p)$ or $r_{\rm QSE}(n)$. From equations (3) and (5) we have

$$Y_{\rm QSE}(p) = \frac{Y_p Y({}^{28}{\rm Si})}{C({}^{28}{\rm Si}) Y_n^{14} Y_p^{14} \prod_{Z'=1}^{13} \{\exp[H_{p,\gamma}(Z')]/\exp[H_{\gamma,p}(Z')]\}}\,. \tag{12}$$

Dividing by Y_p gives

$$\frac{Y_{\rm QSE}(p)}{Y_p} = \frac{Y({}^{28}{\rm Si})}{C({}^{28}{\rm Si}) Y_n^{14} Y_p^{14} \prod_{Z'=1}^{13} \{\exp[H_{p,\gamma}(Z')]/\exp[H_{\gamma,p}(Z')]\}} = \frac{Y_{\rm QSE}(n)}{Y_n}\,. \tag{13}$$

The denominator of equation (13) is identical to the expression for the NSE abundance of ^{28}Si, reflecting the abundance of ^{28}Si if it was in equilibrium with the free nucleons. Thus changes in $r_{\rm QSE}(p)$ [$= r_{\rm QSE}(n)$] reflect the approach of the silicon group to NSE.

4. COMPARISON OF NETWORK RESULTS TO QUASI-EQUILIBRIUM

In Figures 1*a*–1*g* we compare the results of the full network with abundance predictions calculated from the network abundances of *n*, *p*, and ^{28}Si assuming QSE. Elements in QSE will show similar values of $r_{\rm QSE}({}^{A}Z)$ in each of Figures 1*a*–1*g*. Figure 1*a* shows what is a representative pattern when $r_{\rm QSE}({}^{A}Z)$ is plotted against A. From roughly $A = 24$ to $A = 45$, there is a large cluster of nuclei in QSE with ^{28}Si, with a second QSE group stretching from roughly $A = 50$ to the top of the network. Finally, there is a third small group composed of protons, neutrons, α-particles and some other light nuclei. Species in between this lightest group and the silicon QSE group do not form large QSE groups, although they are closer to QSE with silicon than the light-element group. With a temperature of 5×10^9 K,

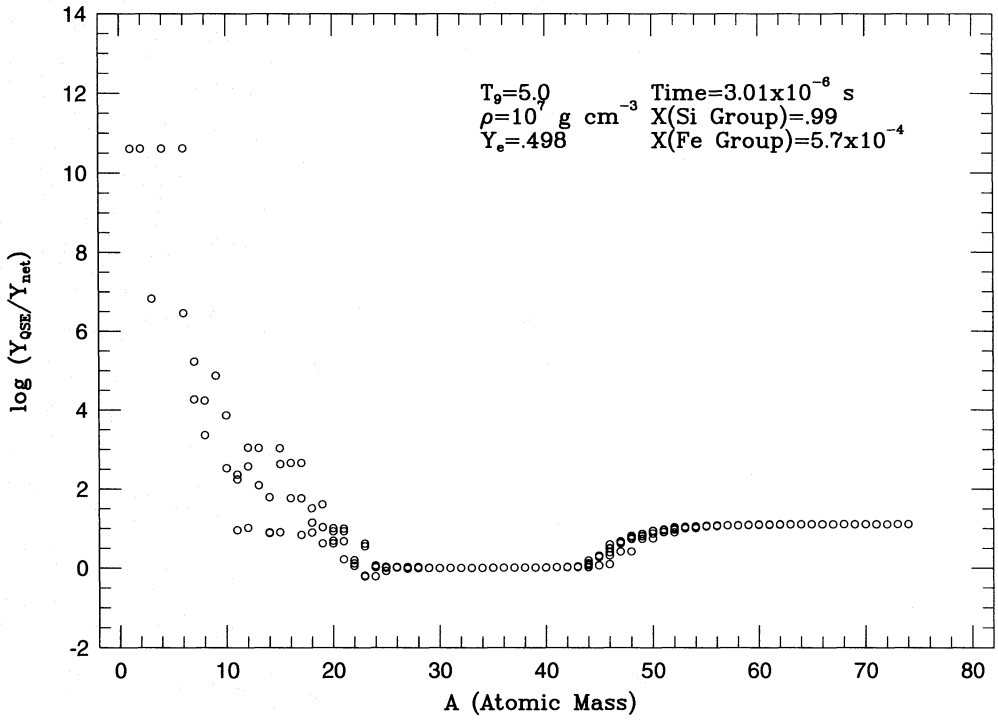

FIG. 1*a*

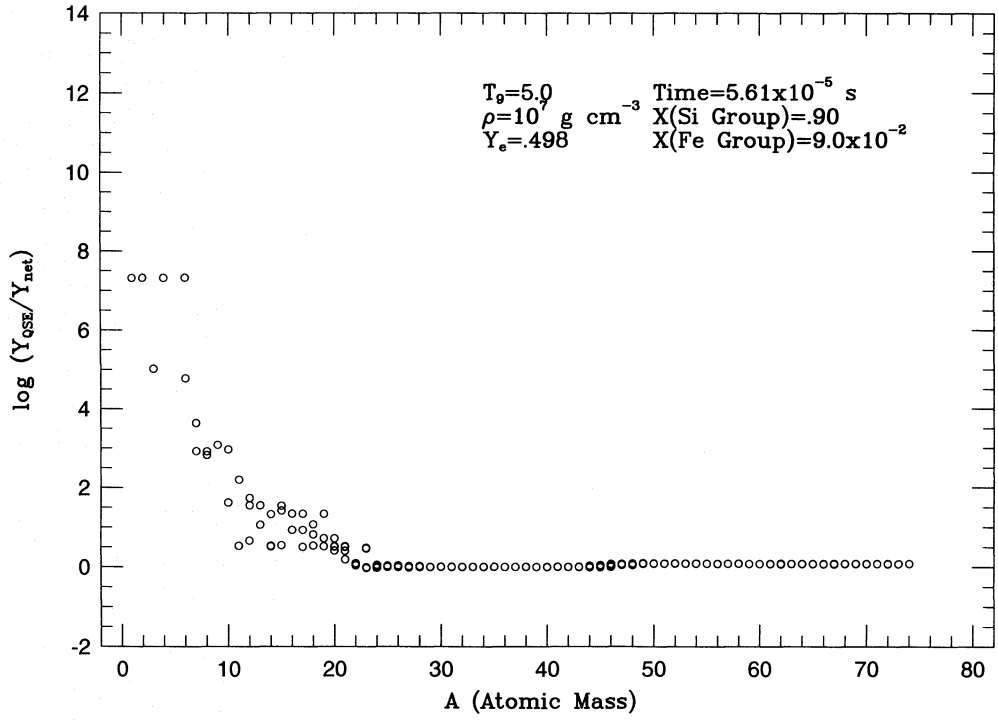

FIG. 1*b*

FIG. 1.—(*a*) Comparison of the silicon QSE abundance to the network abundance, as a function of A, for $T_9 = 5.0$, $\rho = 10^7$ g cm^{-3}, and $Y_e = 0.498$, with X(Si group) = 0.99. (*b*) Comparison of the silicon QSE abundance to the network abundance, as a function of A, for $T_9 = 5.0$, $\rho = 10^7$ g cm^{-3}, and $Y_e = 0.498$, with X(Si group) = 0.90. (*c*) Detail of the comparison of the silicon QSE abundance to the network abundance, as a function of Z, for $T_9 = 5.0$, $\rho = 10^7$ g cm^{-3}, and $Y_e = 0.498$, with X(Si group) = 0.90. (*d*) Comparison of the silicon QSE abundance to the network abundance, as a function of A, for $T_9 = 5.0$, $\rho = 10^7$ g cm^{-3}, and $Y_e = 0.46$, with X(Si group) = 0.90. (*e*) Detail of the comparison of the silicon QSE abundance to the network abundance, as a function of Z, for $T_9 = 5.0$, $\rho = 10^7$ g cm^{-3}, and $Y_e = 0.46$, with X(Si group) = 0.90. (*f*) Detail of the comparison of the silicon QSE abundance to the network abundance, as a function of Z, for $T_9 = 5.0$, $\rho = 10^7$ g cm^{-3}, and $Y_e = 0.46$, with X(Si group) = 0.52. (*g*) Detail of the comparison of the silicon QSE abundance to the network abundance, as a function of Z, for $T_9 = 3.5$, $\rho = 10^9$ g cm^{-3}, and $Y_e = 0.498$, with X(Si group) = 0.90.

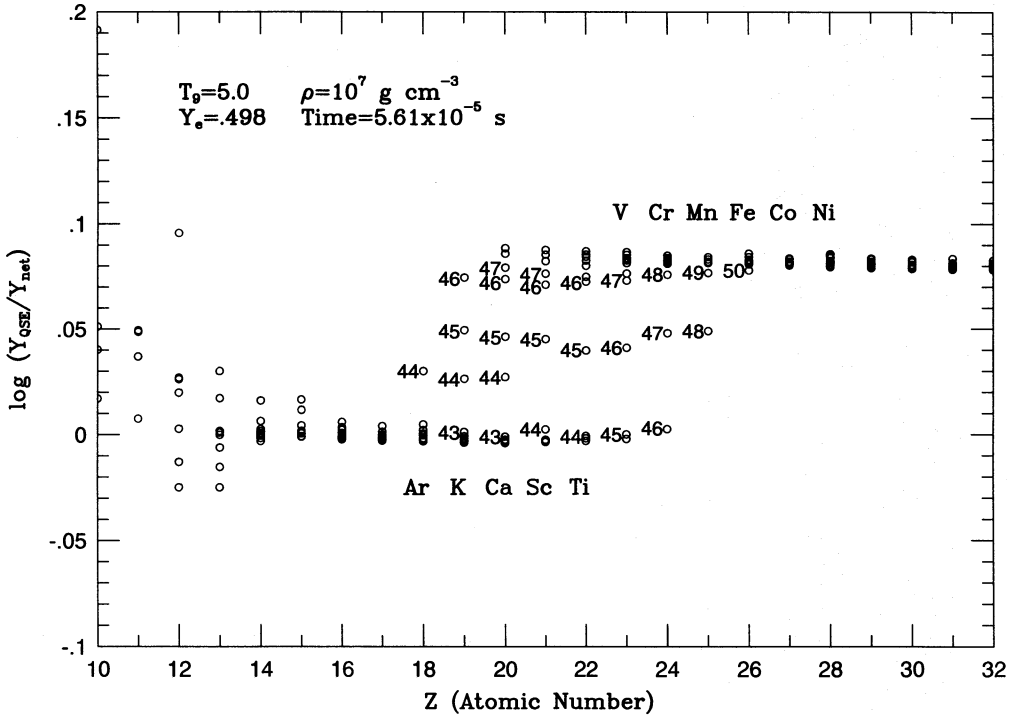

FIG. 1*c*

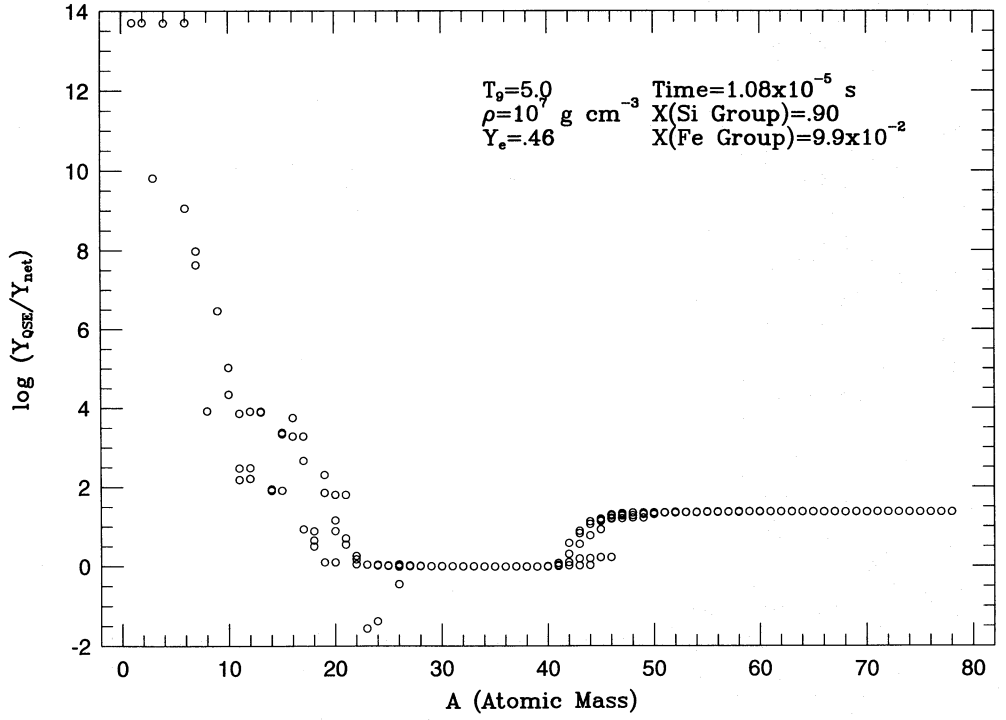

FIG. 1*d*

a density of 10^7 g cm^{-3} and $Y_e = 0.498$, this case is among the fastest we will consider. After an elapsed time of 3.0×10^{-6} s, with 86% of the mass contained in ^{28}Si [$X(^{28}\mathrm{Si}) = 0.86$], and 99% of the mass in the silicon QSE group [X(Si group) = 0.99], QSE is clearly well established. Comparison with Figure 1*b* shows that at a later time [elapsed time = 5.6×10^{-5} s, X(Si group) = 0.90, $X(^{28}\mathrm{Si}) = 0.65$], this pattern is maintained although all nuclei are closer to equilibrium. In fact, all of the nuclei above Na are within 25% of their silicon QSE abundance. However, examination of Figure 1*c*, a detail of Figure 1*b*, plotted now as a function of Z, shows that even within this narrow margin it is still possible to resolve the two QSE groups and a scattering of nuclei between them. Since $r_{QSE}(^4Z)$ is plotted against Z in this figure, with important nuclei labeled by their respective atomic masses, it is also immediately apparent that the boundary between the groups is not as simple as $Z = 21$, since neutron-rich isotopes of K and Ca are

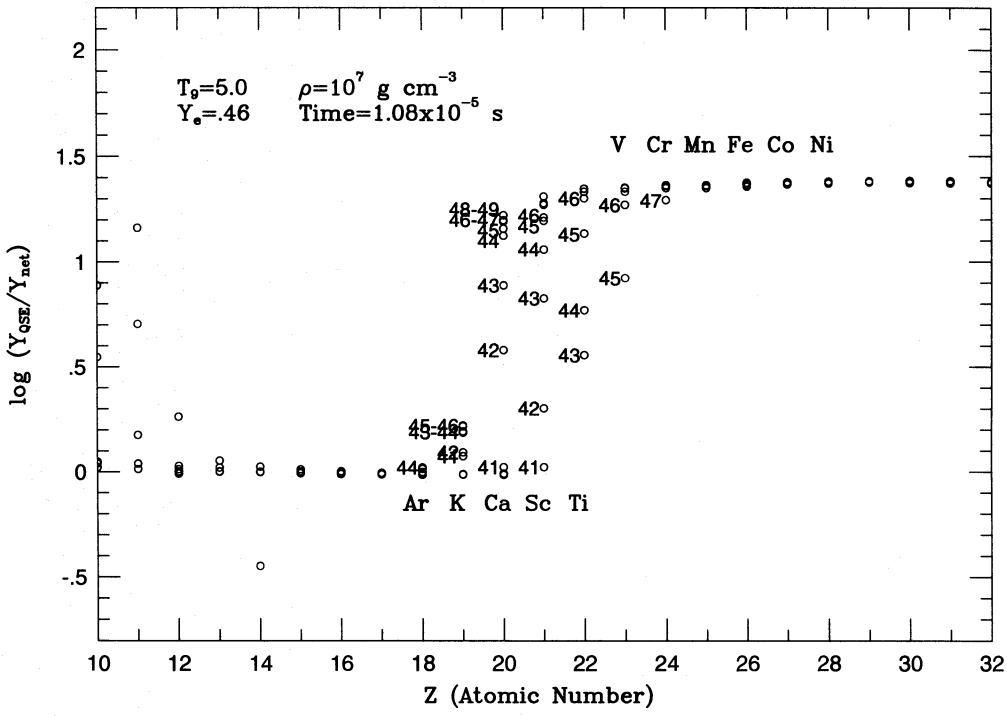

FIG. 1e

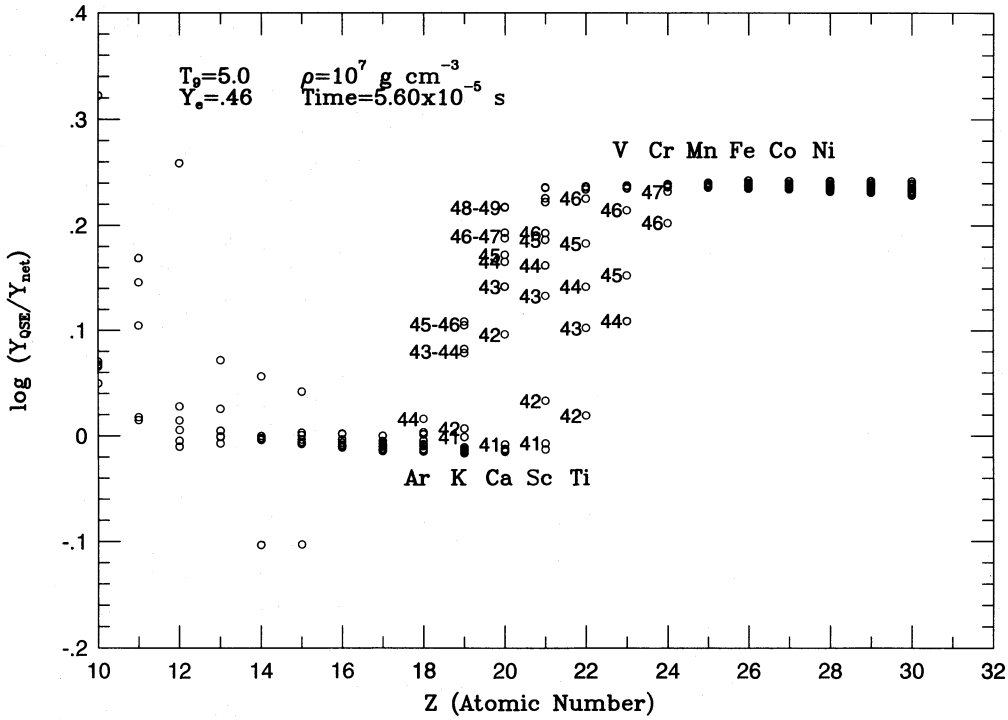

FIG. 1f

clearly members of the upper QSE group, while proton-rich isotopes of V and Cr are in QSE with Si. The description of the boundary as $A = 45$ is more successful, giving way to $N = 23$ from Ti onward. Examination of Table 2 allows a more quantitative comparison of the values of $r_{\rm QSE}(^AZ)$, a point we will return to in a moment. The convergence toward equilibrium continues as time elapses. By an elapsed time of 2×10^{-3} s [X(Si group) = 0.5], the elements that formed the upper group are within 5% of their silicon QSE abundance, even nuclei with mass fractions as small as 10^{-22}.

Previous authors have discussed the progress of silicon burning in terms of the degree of exhaustion of ^{28}Si. For this investigation, where Y_e is a parameter, this description is suspect. The abundance of ^{28}Si in a composition purely of silicon decreases as Y_e decreases. In place of $X(^{28}\text{Si})$, we have chosen to use the mass fraction within the entire silicon QSE group, X(Si group). This choice has several

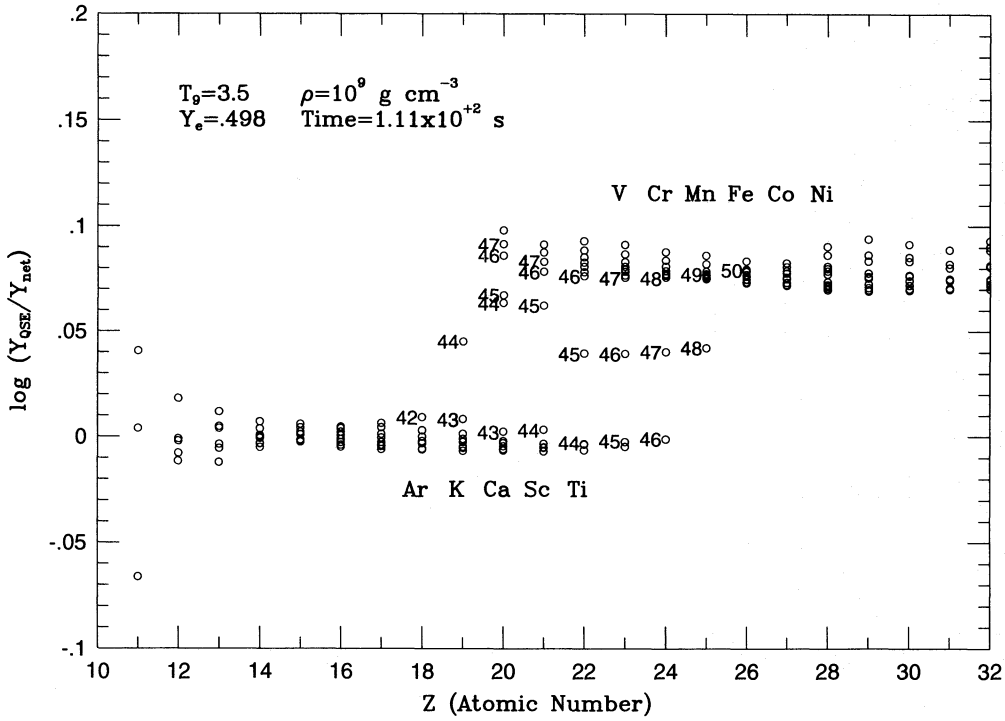

FIG. 1*g*

TABLE 2

QUASI-EQUILIBRIUM FOR SELECTED NUCLEI

	$r_{QSE}(^AZ)$: $T_9 = 5$, $\rho = 10^7$			
SPECIES (1)	$Y_e = 0.498$, $X_{Si} = 0.900$ (2)	$Y_e = 0.46$, $X_{Si} = 0.899$ (3)	$Y_e = 0.498$ $X_{Si} = 0.485$ (4)	$Y_e = 0.46$, $X_{Si} = 0.521$ (5)
^{24}Mg.....	0.026	0.028	0.030	0.028
^{32}S	−0.002	−0.005	−0.003	−0.006
^{36}Ar.....	−0.003	−0.011	−0.006	−0.013
^{43}K.....	0.001	0.187	−0.006	0.079
^{45}K.....	0.049	0.217	−0.003	0.105
^{40}Ca	−0.004	−0.007	−0.008	−0.015
^{42}Ca	−0.002	0.580	−0.009	0.096
^{44}Ca	0.027	1.124	−0.007	0.166
^{46}Ca	0.074	1.191	−0.005	0.188
^{48}Ca	0.086	1.221	−0.003	0.217
^{42}Sc	−0.004	0.302	−0.009	0.033
^{43}Sc	−0.003	0.826	−0.009	0.133
^{44}Sc	0.002	1.058	−0.009	0.162
^{45}Sc	0.045	1.194	−0.008	0.186
^{46}Sc	0.071	1.210	−0.007	0.193
^{47}Sc	0.076	1.270	−0.007	0.222
^{42}Ti	−0.002	...	−0.008	0.019
^{44}Ti	−0.001	0.768	−0.010	0.142
^{45}Ti	0.040	1.134	−0.009	0.183
^{46}Ti	0.072	1.301	−0.009	0.226
^{44}V	−0.002	...	−0.008	0.109
^{45}V	0.000	0.922	−0.009	0.153
^{46}V	0.040	1.270	−0.010	0.215
^{47}V	0.073	1.333	−0.009	0.235
^{46}Cr	0.003	...	−0.009	0.203
^{47}Cr	0.048	1.293	−0.009	0.232
^{48}Cr	0.076	1.349	−0.009	0.239
^{48}Mn.....	0.049	...	−0.009	...
^{49}Mn.....	0.078	1.350	−0.009	0.241
^{50}Fe	0.078	...	−0.008	0.243
^{56}Fe	0.081	1.376	−0.012	0.237
^{58}Fe	0.081	1.375	−0.011	0.236

advantages. Since the mass fraction is dominated by the two QSE groups, the mass fraction within the silicon group does reflect the degree to which material remains to be passed into the upper group (which in NSE will compose 95% or more of the mass). Also, this choice is useful for all Y_e in a way not possible for a single nucleus. This choice is, however, limited in the sense that individual reactions depend on the abundances of individual nuclei. Knowledge of the mass fraction in the silicon group is not sufficient to determine the photodisintegration rate of ^{28}Si, for example. This is an issue which we must keep in mind as we proceed.

As a further demonstration of this difficulty, consider the case where $T_9 = 5.0$, $\rho = 10^7$ g cm^{-3}, but $Y_e = 0.46$. Figure 1*d* is comparable to Figure 1*b*, in the sense that X(Si group) is approximately the same (0.91 for Fig. 1*d* with $Y_e = 0.46$ as compared to 0.90). But the fraction of ^{28}Si differs greatly, with $X(^{28}\text{Si}) = 0.008$ for $Y_e = 0.46$. Furthermore, for $Y_e = 0.46$, $X(^{28}\text{Si})$ is actually rising slightly at X(Si group) ~ 0.9. It should be noted, however, that for $Y_e = 0.46$, X(all isotopes of Si) is 0.64; thus this extremely small abundance of ^{28}Si is specific to this nucleus, and is due to the preference for more neutron-rich nuclei at lower Y_e. There is also considerable difference in the elapsed time, 1.1×10^{-5} s for $Y_e = 0.46$ compared to 5.6×10^{-5} s for $Y_e = 0.498$. Although these elapsed times are small, they are significant, representing the time required to consume 10% of the silicon fuel. Thus such differences in elapsed time are important, implying faster transfer of mass to the iron peak group and consequently, as we will discuss in § 7, a larger energy generation rate. For now, however, the concern is quasi-equilibrium. Comparison of Figure 1*d* with Figure 1*b* shows that the gap between the silicon group and the iron peak group is much larger for $Y_e = 0.46$. Indeed, the underabundance of the iron peak group is more in keeping with that shown in Figure 1*a*. Comparison of Figures 1*c* and 1*e*

reveals that, rather than being 25% underabundant, the nuclei in the QSE group around iron are underabundant by a factor of 25 for $Y_e = 0.46$. This is in spite of the similar fractions of the mass which have been transferred to the iron peak group, 0.09 and 0.1 for $Y_e = 0.498$ and 0.46, respectively. Clearly, the relative underabundance of the iron peak group at low Y_e reflects a much larger QSE abundance for these species rather than an actual dearth of mass transferred. Another point to note in Figure 1*d* is the larger value of $r_{QSE}(p)$ for $Y_e = 0.46$ compared to $Y_e = 0.498$. This reflects the smaller NSE mass fraction of the silicon group (0.00005 for $Y_e = 0.46$, compared to 0.018 for $Y_e = 0.498$), for lower Y_e and hence for the same degree of fuel exhaustion, the composition is further from NSE. These arguments indicate pointedly that the QSE behavior of silicon burning is strongly influenced by the state of neutronization of the material.

Another illustration of the impact of neutronization, which is not easily discernible from Figures 1*b* and 1*d* but is very apparent in Figures 1*c* and 1*e*, is the changing constituents of the QSE groups with declining Y_e. For $Y_e = 0.498$ the distribution is well described as two groups, separated by a narrow fringe of nuclei with $A = 45$ up to Ti and then $N = 23$. The similarity of the value of $r_{QSE}(^4Z)$ for those four species with $N = 23$ (^{45}Ti, ^{46}V, ^{47}Cr, and ^{48}Mn) implies that the reactions linking them are close to being balanced. Comparison of Figures 1*c* and 1*e* reveals a much more complicated pattern. In addition to the vastly different scale, there are many more nuclei in the boundary region. Instead of only a pair of Ca isotopes (^{44}Ca and ^{45}Ca), the isotopes from ^{42}Ca to ^{49}Ca are all significantly displaced from the QSE groups. A similar situation exists for Sc and Ti. Those isotopes of Ti, V, Cr, and Mn which were in the silicon group or the boundary for $Y_e = 0.498$ are significantly closer to the upper group. The nuclei with the largest A which are within a factor of 2 of QSE with the silicon group are ^{42}Sc and ^{46}K. The $N = 23$ nuclei are much closer to the upper group, with ^{47}Cr, for example, having an abundance 20% larger than its iron peak group QSE value as opposed to being a factor of 20 underabundant for QSE with the silicon group. From Ca on, the $N = 22$ and $N = 21$ elements occupy the boundary. The vertical structure of these lines of constant N implies that the reactions linking them, pairs of (p, γ), (γ, p) reactions, are not in equilibrium. Similarly, the spacing of isotopes of Ca, for example, indicates an unbalanced flow by neutron capture upward from the silicon group. We will examine in detail the reaction flows between the groups in § 6. One more interesting note is that, in contrast to the behavior of other nuclei, the neutron-rich isotopes of K (^{44}K, ^{45}K, and ^{46}K), though actually further from their silicon group QSE abundances, seem to be closer to membership in the silicon group. Table 2 shows quantitatively the movement of nuclei upward from the silicon group, with those abundances below the minimum resolution of the network (10^{-25}) represented by (...). Comparison of columns (2) and (3) shows clearly the migration of the boundary toward lower Z and A. The abundance of a nucleus like ^{44}Sc, which for $Y_e = 0.498$ is within 0.5% of its QSE abundance and thus is clearly a member of the silicon group, is, at $Y_e = 0.46$, better predicted by QSE with the iron peak group. For $Y_e = 0.46$ and X(Si group) ~ 0.9, the silicon QSE abundance of ^{44}Sc is over 11 times its network abundance, while its iron peak group QSE abundance is slightly less than half its network abundance. And ^{44}Sc is clearly not an isolated example. Thus the group boundaries defined by earlier work were clearly dependent on the narrow range of parameters examined. We will therefore investigate how our broader range in parameter space effects these boundaries.

One possibility is that the differences in the boundaries are due to the fact that the lower Y_e cases are further from equilibrium. This would result in a temporal variation in the boundary with the boundary discussed above for lower Y_e approaching that of the $Y_e = 0.498$ case at X(Si group) ~ 0.9, as the lower Y_e cases reach a similar degree of convergence. We find that this is not the case. Consider the situations for X(Si group) ~ 0.5. This corresponds to elapsed times of 2.1×10^{-3} and 5.6×10^{-5} s, for $Y_e = 0.498$ and 0.46, respectively, with $T_9 = 5.0$ and $\rho = 10^7$ g cm^{-3}. As column (4) of Table 2 demonstrates, for $Y_e = 0.498$ the abundances of all of the species which composed the iron peak QSE group are within 2%–3% of their silicon QSE abundances. Figure 1*f* illustrates the comparison of the network abundances with those predicted by QSE for $Y_e = 0.46$ and X(Si group) ~ 0.5. The members of the iron peak group are within 50% of their silicon QSE abundances. Comparison of Figures 1*c*, 1*e*, and 1*f* reveals nonetheless that the pattern for $Y_e = 0.46$, X(Si group) ~ 0.5 is more like tht of $Y_e = 0.46$, X(Si group) ~ 0.9, even though the iron peak group has converged much closer to QSE with Si. Although the increased resolution reveals much more detail among the upper members of the boundary, and the isotopes of K continue their slow convergence toward the silicon group, a greater degree of silicon exhaustion leaves the pattern essentially unchanged. While the break which leaves ^{42}Sc and ^{42}Ti, newly emerged from below the minimum mass threshold of the network, close to the silicon group is made more prominent by the approach of these nuclei to the silicon group, the constituents of the QSE groups are essentially unchanged. Furthermore, the dissimilarity of Figures 1*c* and 1*f*, both corresponding to elapsed times of 5.6×10^{-5} s, removes any doubt that the differences in the group boundaries are simply a time dependency. Thus we can conclude that the differences in the boundary between the QSE groups are a genuine effect of the change in Y_e and not due to temporal variation or closeness to equilibrium. As we will discuss in § 7, with the $Y_e = 0.46$ case having exhausted 5 times as much fuel as the similar case with $Y_e = 0.498$ in the same elapsed time, these differences in QSE group structure have broader implications than simply the abundances of these boundary nuclei, resulting in large variations in the rate of energy generation.

Having shown that the QSE behavior during silicon burning is dependent on Y_e and the degree of silicon exhaustion, we now turn to our two remaining parameters. The conditions considered so far, high temperature and low density, are the most like those considered by WAC. They are also the conditions under which the inclusion of screening is the least critical. For conditions like those of Figure 1*g*, $T_9 = 3.5$ and $\rho = 10^9$ g cm^{-3}, the inclusion of screening in the QSE is very important. Under these conditions the screening portion of equation (4) can be as large as 10^6, much larger than the factor of 5 which is the maximum for $T_9 = 5.0$ and $\rho = 10^7$ g cm^{-3}, but much smaller than the factor of order 10^{13} which is possible for $T_9 = 3.5$ and $\rho = 10^{10}$ g cm^{-3}. Comparison of Figures 1*c* and 1*g* supports the inclusion of this screening term. With $Y_e = 0.498$ and X(Si group) = 0.9, the conditions of Figure 1*g* differ

from the conditions of Figure 1*c* only in temperature and density. Since the screening term is dependent on Z and not on N, its omission would result in a separate horizontal line for each element, with Ge being displaced from Si by a factor of almost 10^6. The similarity of Figures 1*c* and 1*g* argues strongly that the inclusion of screening is correct. This similarity also argues that the changes of temperature and density do not strongly affect the structure of the QSE groups, although the elapsed time, 111 s, is considerably different, reflecting the much slower reaction rates at low temperatures. The most striking difference between these cases is the larger values of $r_{\rm QSE}(^AZ)$ among the lighter nuclei. The much greater value of $r_{\rm QSE}(p)$ (16.92 compared with 7.32) for this low-temperature/high-density case is consistent with the argument that $r_{\rm QSE}(p)$ reflects how far from NSE the distribution is. Since the NSE mass fraction of the silicon group for these conditions is less than 2×10^{-5}, the smallest of the cases shown in this paper, one would expect $r_{\rm QSE}(p)$ for this degree of silicon exhaustion to be the largest in this case.

Clearly changes in temperature and density affect the reaction rates, and hence timescales, but how does this affect adherence to the QSE distributions? Comparison of Figure 1*g* with Figure 1*c* shows that, for $Y_e = 0.498$, the variation of temperature and density has little effect on the QSE group behavior. Once again, for X(Si group) = 0.9, the members of the iron peak group are within 25% of their silicon QSE group abundances. The spread within the iron peak group is noticeably larger, but still less than approximately 5%. Further investigation reveals that this greater disorder, i.e., larger variation within the QSE groups, is solely a function of decreasing temperature. Most important, although there is some difference in relative placement, the nuclei intermediate between the two QSE groups are the same. Examination of cases with lower Y_e supports the finding that the variation of temperature and density does not affect the grouping of nuclei, although it can radically alter relative abundances among the collection intermediate to the QSE groups.

While previous authors have shown the value of QSE as a key to understanding the process of silicon burning, the work presented in this section implies that this understanding is incomplete. As one might expect, variation of the temperature or density can produce large differences in the behavior of silicon burning, most notably in the timescale. The important result of this research is the importance of neutronization in the QSE behavior and timescale. For similar degrees of silicon exhaustion, a decrease in Y_e results in a drastic increase in the QSE abundances of the iron peak group. As a result, for similar degrees of silicon exhaustion the iron peak group is much farther from QSE and the abundances of these nuclei a much smaller fraction of their silicon QSE abundance. This delays the merging of the two QSE groups into a single group spanning the elements from Mg to Ge. While high Y_e cases reach this merged group stage with approximately 90% of the mass remaining within what was the silicon group, for lower Y_e this mass fraction is much smaller. For $Y_e = 0.498$, for both $T_9 = 5.0$, $\rho = 10^7$ g cm^{-3} and $T_9 = 3.5$, $\rho = 10^9$ g cm^{-3}, a single QSE group (within 10%) has formed by X(Si group) = 0.85. For $Y_e = 0.48$ the iron peak nuclei do not reach 90% of their silicon QSE group abundance until 50% or more of the mass in the silicon group is exhausted. At $Y_e = 0.46$, for $T_9 = 5.0$, $\rho = 10^7$ g cm^{-3} and $T_9 = 3.5$, $\rho = 10^9$ g cm^{-3}, the iron peak group reaches 90% of its silicon QSE abundance with silicon group mass fractions of 0.25 and 0.3, respectively. Although variations of temperature and density clearly effect great changes in the timescales of silicon burning, it is the degree of neutronization which most strongly affects the QSE behavior. This behavior, previously only hinted at by TA, is very important to modeling the mechanism of silicon burning, since low Y_e results in the persistence of two separate QSE groups until much later than previously thought. Attempts, like that of BCF, to model silicon burning by using the QSE abundances and calculating the loss from a single QSE group, are, as a result, oversimplified. Our results show that such a method would be inaccurate unless this separation between the upper and lower QSE groups is included, as the gap can persist through significant silicon consumption, causing larger miscalculations in the iron peak abundances.

Furthermore, for smaller Y_e, the upper boundary of the silicon group moves downward, while at the same time the nuclei which formerly comprised the boundary layer have, for the most part, joined the iron peak group. This movement of the boundary has a number of effects, the most important being that it mandates there be different reactions which link the QSE groups as Y_e varies. It is hard to see how the reaction ^{45}Sc$(p, \gamma)^{46}$Ti can be the link between QSE groups for $Y_e = 0.46$, since ^{45}Sc is virtually a member of the iron peak group under these conditions. The similarity in $r_{\rm QSE}(^AZ)$ for ^{45}Sc and ^{46}Ti for $Y_e = 0.46$ implies that the (p, γ), (γ, p) reaction pair linking them are almost balanced, making this an unlikely flow path. In § 6 we will investigate the question of how the linking reactions vary as conditions change, but first we will use the convenience of QSE to follow the nuclear abundances produced during silicon burning.

5. SPECIES FORMATION DURING SILICON BURNING

The applicability of QSE greatly simplifies the study of the nuclei produced by silicon burning. Instead of following the intricacies of the production of 300 nuclei, much can be learned by examining four: free protons, free neutrons, and one member of each of the QSE groups. While the focal members of the QSE groups map the spacing between the groups, it is the abundances of the free particles which control the relative abundances within the QSE groups. The gap between QSE groups, seen in Figures 1*a*–1*g*, which diminishes as silicon approaches exhaustion, reflects the evolution of the focal elements of the QSE groups. Figure 2 shows samples of the evolution of the free-proton and free-neutron mass fractions as a function of time. Although the actual abundances vary by many orders of magnitude, comparison with the appropriate NSE abundances reveals a similarity in pattern. For each of the cases portrayed in Figure 2, $T_9 = 5.0$, $\rho = 10^7$ g cm^{-3}, and $Y_e = 0.498$ (*solid lines*), $T_9 = 5.0$, $\rho = 10^9$ g cm^{-3}, and $Y_e = 0.48$ (*dotted lines*), and $T_9 = 3.5$, $\rho = 10^9$ g cm^{-3}, and $Y_e = 0.46$ (*dashed lines*), the pattern is similar. Although the rates of convergence vary greatly, in each case the network abundance of free photons is initially more than an order of magnitude smaller than its equilibrium abundance and converges gradually to equilibrium as the mass fraction of the silicon group approaches its equilibrium value. The behavior of the neutrons is slightly more complicated. These abundances begin more than an order of magnitude larger, than their equilibrium abundance, and converge down toward equi-

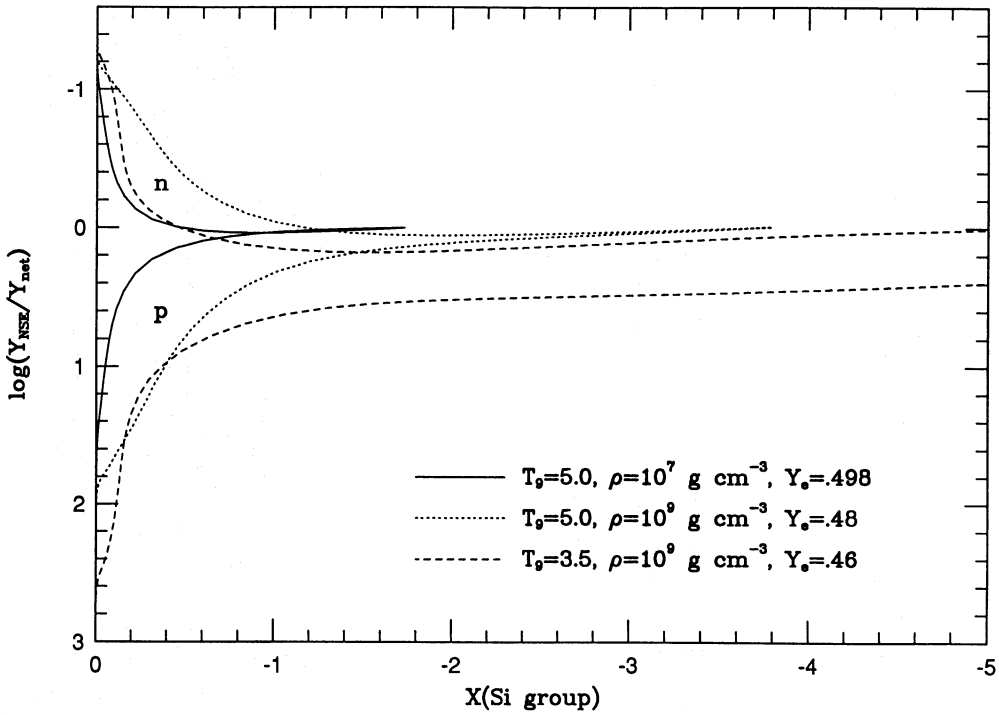

FIG. 2.—Convergence of the free-nucleon abundances to equilibrium as a function of degree of silicon exhaustion. The cases portrayed are $T_9 = 5.0$, $\rho = 10^7$ g cm^{-3}, and $Y_e = 0.498$ (*solid lines*); $T_9 = 5.0$, $\rho = 10^9$ g cm^{-3}, and $Y_e = 0.48$ (*dotted lines*); and $T_9 = 3.5$, $\rho = 10^9$ g cm^{-3}, and $Y_e = 0.46$ (*dashed lines*).

librium, briefly becoming underabundant before reaching equilibrium. As with the protons, the details of this behavior—the rate of convergence, the maximal and minimal abundances, and the equilibrium mass fractions—vary widely. But this simple pattern is maintained. What effect do such variations have? The relative abundance of two isotopes of a given element are related by

$$\frac{Y_{\rm QSE}(^{A'}Z)}{Y_{\rm QSE}(^{A}Z)} \propto Y_n^{(A'-A)} . \qquad (14)$$

Thus an overly large neutron abundance tips the production of an element toward more neutron-rich isotopes. Clearly this occurs because the increased neutron abundance increases the rate of neutron capture. Similarly the dearth of free protons will favor the enhancement of the members of a QSE group with lower atomic number. Figure 3*a* shows the evolution of the abundances for key members of the iron peak group as the degree of silicon exhaustion increases for $T_9 = 5.0$, $\rho = 10^7$ g cm^{-3}, and $Y_e = 0.498$. For comparison, the corresponding evolution of the free nucleons is shown as the solid line in Figure 2. At early time [X(Si group) ~ 0.9)], the iron peak group is dominated by ^{54}Fe and ^{56}Fe. As X(Si group) decreases, the abundance of ^{54}Fe levels out while ^{56}Fe actually decreases in abundance as the overabundance of free neutrons drops. Meanwhile, as the free-proton abundance rises toward equilibrium, ^{56}Ni and ^{58}Ni rise to prominence. This results in temporal variations in the relative abundances of the nuclei which dominate the distribution. It is not until very late that ^{56}Ni, which is the most abundant nucleus in the NSE distribution for these conditions, becomes most abundant in the network distribution. The relative abundances of ^{54}Fe, ^{56}Fe, and ^{58}Ni at X(Si group) ~ 0.9 are similar to those found in the NSE distribution for $Y_e \sim 0.475$. At X(Si group) ~ 0.5, the relative abundances of ^{54}Fe, ^{56}Ni, and ^{58}Ni are comparable to those found in NSE for $Y_e \sim 0.49$. In another similarity to the NSE distribution, nuclei with similar Z/A react in concert. For example, the abundances of ^{56}Fe and ^{60}Ni react to a decreasing silicon group mass fraction by rising sharply, peaking around X(Si group) ~ 0.9, and then falling off. For ^{56}Fe this shallow decline turns around for X(Si group) ~ 0.1, coincident with the minimum of the free-neutron distribution. As the free neutrons converge back toward their equilibrium value, the abundance of ^{56}Fe also increases slightly. For ^{60}Ni this decline after maximum is turned around for X(Si group) ~ 0.4 as the increase in the free-proton fraction overcomes the decline in the free-neutron fraction. Even after the abundance of ^{56}Fe begins to increase again, the rate of increase in the abundance of ^{60}Ni, aided by its greater dependence on the free-proton abundance, is greater. Other such pairings of nuclei observed in the NSE distributions, like ^{54}Fe and ^{58}Ni or ^{58}Fe and ^{62}Ni, also behave in concert.

This excessive neutron richness of the iron peak group at early times is also apparent for other thermodynamic conditions. For $T_9 = 5.0$, $\rho = 10^9$ g cm^{-3}, and $Y_e = 0.48$, shown in Figure 3*b* (and as the dotted line in Fig. 2), the relative distribution of ^{54}Fe, ^{56}Fe, ^{58}Ni, and ^{60}Ni, at X(Si group) ~ 0.5, is more in keeping with equilibrium distributions with $Y_e \sim 0.47$. Once again, relatively neutron-rich isotopes, in this case ^{58}Fe, ^{60}Ni, and ^{62}Ni, peak early, exhibit a local minimum in concert with a similar local minimum in the abundance of free neutrons, and then rise toward equilibrium. Here again, the increasing abundance of free protons causes the Ni isotopes to rise more quickly than their Fe brethren. Thus the behavior of this example is consistent with the previous case, though even more neutron-rich, as one might expect from this lower Y_e case.

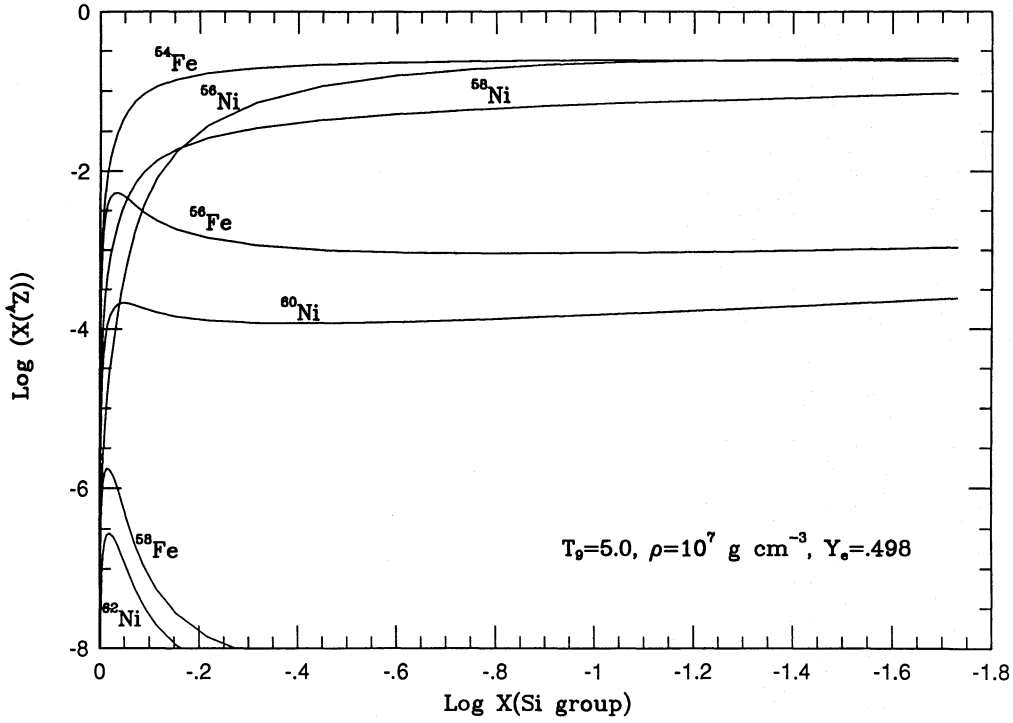

FIG. 3a

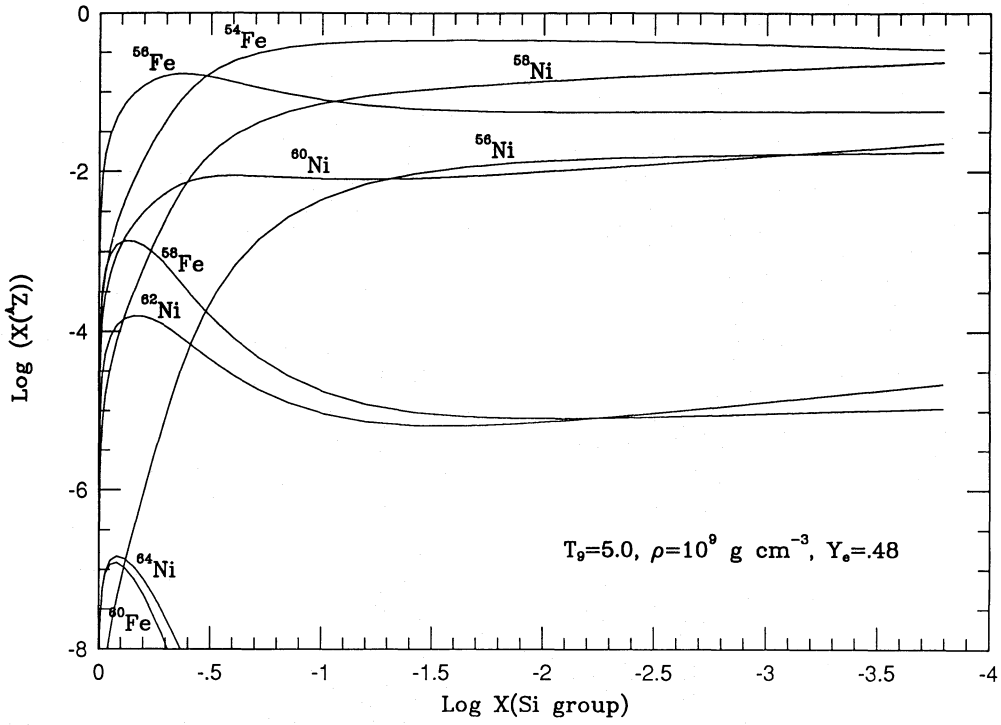

FIG. 3b

FIG. 3.—(*a*) Evolution of the mass fractions of the dominant members of the iron peak group as a function of the degree of silicon exhaustion for $T_9 = 5.0$, $\rho = 10^7$ g cm^{-3}, and $Y_e = 0.498$. Compare with the solid line in Fig. 2. (*b*) Evolution of the mass fractions of the dominant members of the iron peak group as a function of the degree of silicon exhaustion for $T_9 = 5.0$, $\rho = 10^9$ g cm^{-3}, and $Y_e = 0.48$. Compare with the dotted line in Fig. 2. (*c*) Evolution of the mass fractions of the dominant members of the iron peak group as a function of the degree of silicon exhaustion for $T_9 = 3.5$, $\rho = 10^9$ g cm^{-3}, and $Y_e = 0.46$. Compare with the dashed line in Fig. 2.

For $T_9 = 3.5$, $\rho = 10^9$ g cm^{-3}, and $Y_e = 0.46$, shown in Figure 3*c* (and as the dashed line in Fig. 2), the early behavior is even more neutron-rich. For X(Si group) ~ 0.5, the relative distribution of ^{56}Fe, ^{58}Fe, ^{60}Ni, and ^{62}Ni reflects a $Y_e < 0.45$. Even for material which is highly neutronized, the iron peak group is especially neutron-rich at early times.

Over this wide range of conditions, the abundance distributions within the iron peak group exhibit a number of similarities. First, the relative abundances are very reflective of the changes in the free-nucleon abundances. Second, at early times, particularly when the silicon group still dominates the mass fraction, the iron peak group exhibits a

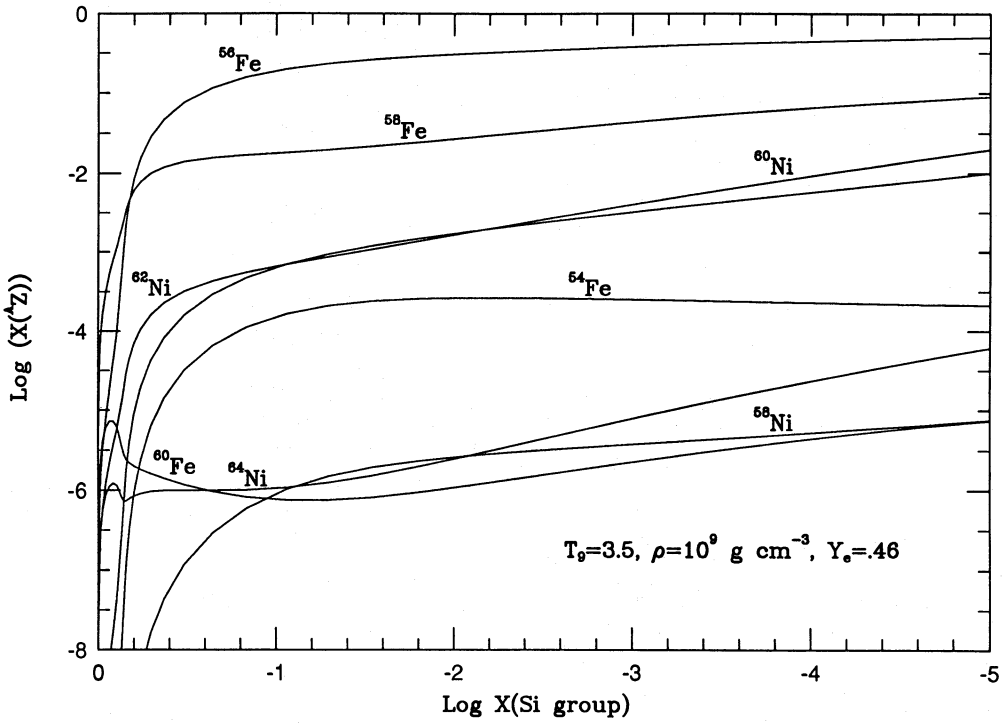

FIG. 3c

higher degree of neutronization than the abundance distribution as a whole. The solid line in Figure 4, which plots the average Z/A of the iron peak group as the degree of silicon exhaustion increases, for $T_9 = 5.0$, $\rho = 10^9$ g cm^{-3}, and $Y_e = 0.48$ (the same conditions as in Fig. 3*b*), shows that this excessive neutronization is not an illusion of the most abundant nuclei. For the iron peak group to show excessive neutronization, there must be a group of nuclei which are neutron poor relative to the global Y_e. This is required by the constancy of total neutron number in the absence of weak interactions. Since the mass fractions of the light particles are very small, the likely source of these excess neutrons is the silicon group. The dotted line in Figure 4, which shows the average Z/A for the silicon group as it is depleted, vindicates this assertion. Clearly, in equilibrium, the neutron richness of the silicon group is much lower than the global neutronization indicates. While in small part this is due to the absence of the most neutron-rich isotopes of Ca,

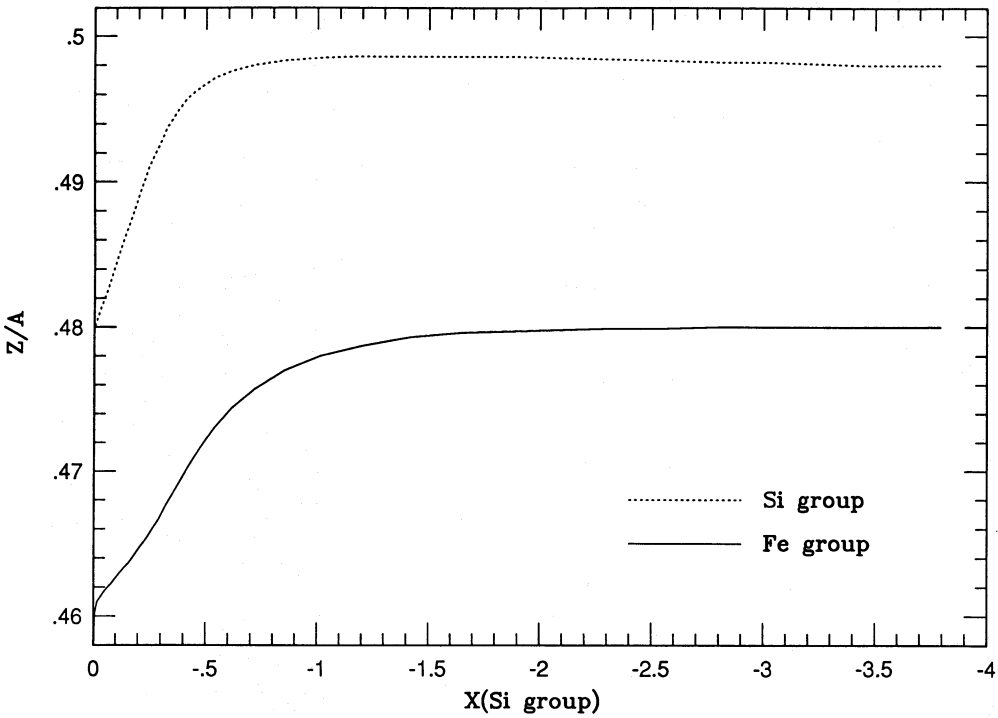

FIG. 4.—Evolution of the average Z/A for the iron peak group (*solid line*) and the silicon group (*dotted line*) with the degree of silicon exhaustion for $T_9 = 5.0$, $\rho = 10^9$ g cm^{-3}, and $Y_e = 0.48$. Compare with Fig. 3*b*.

TABLE 3

AVERAGE Z/A AS A FUNCTION OF ELEMENT IN NSE AT $T_9 = 5.0$, $\rho = 10^9$ g cm^{-3}, AND $Y_e = 0.48$

Element	Z/A	Element	Z/A	Element	Z/A
n.....	0	Na	0.479	Ti	0.477
H.....	1	Mg.....	0.500	V.....	0.473
He.....	0.500	Al	0.482	Cr.....	0.474
Li	0.500	Si	0.500	Mn.....	0.473
Be	0.548	P.....	0.485	Fe.....	0.478
B	0.464	S	0.498	Co	0.481
C	0.500	Cl	0.486	Ni.....	0.483
N.....	0.500	Ar.....	0.496	Cu	0.480
O.....	0.500	K	0.487	Zn	0.480
F	0.528	Ca	0.499	Ga	0.478
Ne.....	0.500	Sc.....	0.481	Ge	0.477

Sc, and Ti from the silicon group, the major cause is the relative binding energies within the silicon group.

As Table 3 indicates, under conditions of NSE, even with $Y_e = 0.48$, elements which compose the silicon group are dominated by their $N = Z$ isotopes. This is particularly true for the dominant elements, Si, S, Ar, and Ca, where the $N = Z$ isotope is also an α-nucleus. As for nuclei with Z between 2 and 10, the valley of maximal binding energy is narrow for elements within the silicon group. With the high temperatures of silicon burning, and the resultant photon distribution, the more neutron-rich isotopes within the silicon group, with binding energies smaller than their $N = Z$ neighbors, are more quickly photodissociated, freeing large numbers of free neutrons. These neutrons are captured by nuclei in the iron peak group, where the binding energy valley has curved to the neutron-rich side and widened, and thus the neutron-rich isotopes are more durable. Thus it is the tendency toward $N = Z$ nuclei within the silicon group which fuels the extreme neutron excesses in the iron peak group during silicon burning. This provides a mechanism for producing small quantities of more neutron-rich iron peak group nuclei, characteristic of a larger η. As Figure 4 shows for $T_9 = 5.0$, $\rho = 10^9$ g cm^{-3}, and $Y_e = 0.48$, if only 10% of the silicon was exhausted, the effective η within the iron peak group would be 0.08, twice its equilibrium value. Thus, by such a mechanism it is possible to produce neutron-rich members of the iron peak group from material which has never experienced the high densities necessary to produce such a large global neutron excess. By tying up the bulk of the nucleons in $N = Z$ nuclei, and thereby amplifying the effective neutronization among the iron peak nuclei, incomplete silicon burning faintly echoes the emerging understanding of the r-process (see Woosley & Hoffman 1992). This neutron enrichment of the iron peak group is clearly a consideration when one is modeling objects where explosive burning of silicon, and hence incomplete silicon burning, are important to the elemental production.

6. REACTION FLOWS

With the majority of the mass concentrated within the two QSE groups, the process of silicon burning is dominated by these groups of nuclei. The previous section indicates that, with knowledge of the free-nucleon abundances, it is possible to ignore the reactions within the QSE groups, since these reactions simply reflect the changes in abundances required for nuclei to remain in QSE under changes in the free-proton and free-neutron fractions. Thus, instead of studying the thousands of reactions which make up silicon burning, we can concentrate on those reactions which enter or leave the QSE groups. Ideally, these few important reactions would be the same for all physical conditions. However, in § 5 we demonstrated that small changes in neutronization result in much larger changes in the free-neutron abundance, thus favoring neutron capture and more neutron-rich nuclei. This enhanced importance of neutron captures affects the boundary region and results in changes in the location of the boundaries of the silicon and iron peak QSE groups, as we discussed in § 4. As a result we expect that the dominant reactions linking these groups must change as a function of Y_e. However, before we examine the complicated behavior that joins the silicon and iron peak groups, let us examine the lower boundary condition for the QSE groups.

6.1. *Downward Flows from Silicon*

While we have heretofore concentrated on the upper edge of the silicon QSE group, the flow from the lower edge is also important to the destruction of silicon and the other constituents of the silicon group. Previous authors have shown that these reactions govern the rate at which silicon is destroyed. Examination of Figures 1*a*, 1*b*, or 1*d* shows that the network abundances of the nuclei below $A \sim 24$ are orders of magnitude less than their silicon QSE abundances, with the degree of underabundance increasing as Z decreases. Further, there is little evidence of QSE behavior among these nuclei. Figures 1*c* and 1*e* reveal that the principal isotopes of Mg and Al are close to their silicon QSE abundances. Within a margin of $\pm 10\%$, all of the isotopes of Mg and Al, except ^{21}Mg and perhaps ^{22}Mg, are members of the silicon group. This closeness to QSE does not hold for Na and Ne. Thus the bottom edge of the silicon group is Mg. If the principle isotopes of Mg and Al are in QSE with ^{28}Si, then the rate of photodissociation of ^{28}Si, either by ^{28}Si(γ, α)^{24}Mg or by ^{28}Si(γ, p)^{27}Al, is essentially balanced by the reverse capture reactions. Thus it is the net flow from this bottom edge which governs the downward flow from silicon. BCF contended that, with ^{24}Mg in QSE with ^{28}Si, the rate of destruction of ^{28}Si was governed by the photodissociation of ^{24}Mg, with ^{24}Mg(γ, α)^{20}Ne dominating ^{24}Mg(γ, p)^{23}Na. This was supported by WAC, who found that these reactions did indeed dominate the downward flow. However, the reaction network used by WAC was very narrow at this lower boundary of the silicon group with four isotopes of Mg, and only single isotopes of Al, Na, and Ne. Further, because of doubt over the accuracy of the then best available reaction rates, a number of reactions which those authors described as potentially important, like ^{24}Mg(p, α)^{21}Na and ^{24}Mg(n, α)^{21}Ne, were excluded from their reaction network. Thus we now reexamine the reactions which cross this lower boundary to see the importance of our improved reaction network in addition to examining the effects of the range of Y_e.

While the variation of Y_e has considerable influence on the relative abundances of the Mg isotopes, there is not the pronounced shift in group membership at this lower boundary that exists at the upper boundary. Comparison of Figures 1*c*, 1*f*, and 1*g* shows changes in the relative spacing of the Mg isotopes, and a somewhat more pronounced spread in those cases further from NSE, but little evidence of significant movement of the lower boundary. Thus the

effects of variation of Y_e on the lower boundary are simply changes in relative abundances. Since changes in Y_e have no counteracting effect on the reaction cross sections, these changes in relative abundances significantly alter the reaction balances. In this and the following subsection, we will show a series of vector diagrams of the integrated reaction fluxes, forward reaction rate minus its respective reverse, integrated over time. The direction of the vector reflects the dominant reaction of the pair, pointing from target to product. In order to show best the many reactions which contribute and yet in which the dominant vectors are not visually overwhelming, the magnitudes of these vectors have a logarithmic dependence on the actual magnitude of the flux. As an example, in Figure 5*a*, for $T_9 = 5.0$, $\rho = 10^7$ g cm^{-3}, and $Y_e = 0.498$, the flux through ^{24}Mg(γ, α)^{20}Ne is 12 times greater than that through ^{23}Mg(n, α)^{20}Ne, though the vector representing ^{24}Mg(γ, α)^{20}Ne is only 1.4 times longer than the vector representing ^{23}Mg(n, α)^{20}Ne. Figure 5*a* shows the reaction fluxes integrated from X(Si group) = 0.95 to 0.5, which is the portion of the burning where the boundary between the silicon group and elements of lower Z is most important. Even at X(Si group) = 0.5, the abundances of ^{23}Na and ^{20}Ne are less than 0.5 and 0.6 of their respective silicon QSE abundances. As expected, the downward flows from the silicon group strongly dominate mass transfer across this border. Only a few small fluxes, most notably ^{22}Na(n, p)^{22}Mg and ^{22}Na(α, n)^{25}Al, point upward across the boundary. At first glance, this figure also seems to agree with the results of WAC, with the flux through ^{24}Mg(γ, α)^{20}Ne being nearly 3 times the flux through ^{24}Mg(γ, p)^{23}Na. But the largest reaction flux downward from the silicon group is actually ^{26}Mg(p, α)^{23}Na, with a flux 5.3 times larger than that through ^{24}Mg(γ, p)^{23}Na. In addition, there is a group of lesser flows, including ^{24}Mg(p, α)^{21}Na, ^{23}Mg(n, p)^{23}Na, ^{23}Mg(n, α)^{20}Ne, and ^{26}Al(n, α)^{23}Na, which in sum rival the importance of ^{24}Mg(γ, α)^{20}Ne. This is certainly more complicated than the simple approach taken by BCF. Thus our more extensive network indicates that the apparent simplicity of the results of BCF and WAC is due to limitations in their calculation.

This is further reinforced by examination of the reaction fluxes for lower Y_e. In Figure 5*b*, identical to Figure 5*a* except that $Y_e = 0.46$, the reactions ^{24}Mg(n, α)^{21}Ne, ^{26}Mg(p, α)^{23}Na, ^{25}Mg(n, α)^{22}Ne, ^{23}Mg(n, p)^{23}Na, ^{23}Mg(n, α)^{20}Ne, and ^{24}Mg(n, p)^{24}Na all carry more flux than ^{24}Mg(γ, α)^{20}Ne. This tendency at lower Y_e to favor reactions with neutrons in the incoming channel and neutron-rich nuclei as targets is very much in keeping with the much larger free-neutron abundances found for these conditions. There is also a noteworthy flux upward via ^{23}Na(α, n)^{26}Al. This flux is actually part of a cycle, ^{23}Na(α, n)^{26}Al(n, p)^{26}Mg(p, α)^{23}Na, with the flux through ^{23}Na(α, n)^{26}Al representing less than 7% of the flux through ^{26}Mg(p, α)^{23}Na. It is a myriad of cycles like this within the QSE groups which keeps the α-particles in equilibrium with the free nucleons.

Variations of temperature and density do not cause strong changes in the relative importance of reactions like those due to variations of Y_e. Figure 5*c*, with $T_9 = 3.5$, $\rho = 10^9$ g cm^{-3}, and $Y_e = 0.498$, is similar to Figure 5*a*. In this case ^{24}Mg(γ, α)^{20}Ne does actually carry the largest flux, but the same reactions we found important in Figure 5*a* are also important here. Thus the variation of temperature, which alters the balance of each set of forward and reverse reactions, and density, which enhances captures, can result in differences in relative fluxes, but in general does not open up drastically different paths, since these variations do not result in the large free-neutron fraction found to be important for low Y_e. With the passage of time and the approach to equilibrium, the reaction flows dwindle. The approach to equilibrium also implies that the isotopes of Na and Ne are not as underabundant. Thus the dominance of the flows downward from the silicon group over those flows directed upward lessens. This is illustrated in Figure 5*d*, which presents the integrated flux from X(Si group) = 0.1 to X(Si group) = 0.02, for $T_9 = 5.0$, $\rho = 10^7$ g cm^{-3}, and $Y_e = 0.498$. Over the corresponding interval of time, the abundance of ^{20}Ne converges from 80% of its QSE abundance to its NSE value. The sum of the upward fluxes, principally ^{21}Na(α, p)^{24}Mg, is almost as large as the sum of the downward fluxes. Furthermore, the balances between some pairs of reactions have changed. Representative of this trend, the balance of ^{21}Ne(α, n)^{24}Mg and ^{24}Mg(n, α)^{21}Ne, which favored ^{24}Mg(n, α)^{21}Ne at early times, favors ^{21}Ne(α, n)^{24}Mg as equilibrium is approached.

Thus the use of our larger and improved network indicates that there are a number of reactions, in addition to the photodisintegration reactions of ^{24}Mg, which are important to understanding the depletion of the silicon group toward lighter nuclei. Under some conditions, particularly low Y_e, these alternative reactions dominate the ^{24}Mg(γ, α)^{20}Ne and ^{24}Mg(γ, p)^{23}Na reactions which previous authors found to be the most important. We do agree with previous authors in finding that, as equilibrium is approached, the decreasing abundance of the Mg isotopes, mandated by QSE, and the closer proximity of the Ne and Na isotopes to their silicon QSE abundances, results in a decline in the net flux of mass downward from the silicon group. This equilibration of the lighter nuclei with the silicon group is the final phase of silicon burning, occurring well after the abundances are dominated by the iron peak elements and a single QSE group stretches upward from Mg. By this point, as we will show in §§ 6.2 and 7, the conversion of silicon into iron peak elements no longer dominates the energy production but serves as a source of free particles, driving the distribution to NSE.

6.2. *Bridging the Gap between Silicon and Iron*

While the downward flow from the silicon group generates the free nucleons needed to build silicon into iron peak elements, and hence governs the timescale for silicon burning, the links between the silicon and iron peak QSE groups mediate the formation of the iron peak. For times prior to the establishment of a single QSE group, a small number of reactions dominate the flow into the iron peak group. It is the slowness of these reactions which allows the persistence of two separate groups. WAC found that, with their network, the flow was dominated by a group of reactions ending in ^{46}Ti. They contended that the dominant flow was ^{45}Sc(p, γ)^{46}Ti, aided at high temperature by ^{42}Ca(α, γ)^{46}Ti and ^{45}Ti(n, γ)^{46}Ti. This contradicted earlier work by BCF and Michaud & Fowler (1972), which had selected ^{44}Ti(α, p)^{47}V as the principal bridge. WAC argued that this reaction was only important at late times when a single QSE group was a good approximation. We will examine both of these contentions within the context of our larger network, and also examine the influence of Y_e, something not done by previous authors.

For $T_9 = 5.0$, $\rho = 10^7$ g cm^{-3}, and $Y_e = 0.498$, we find

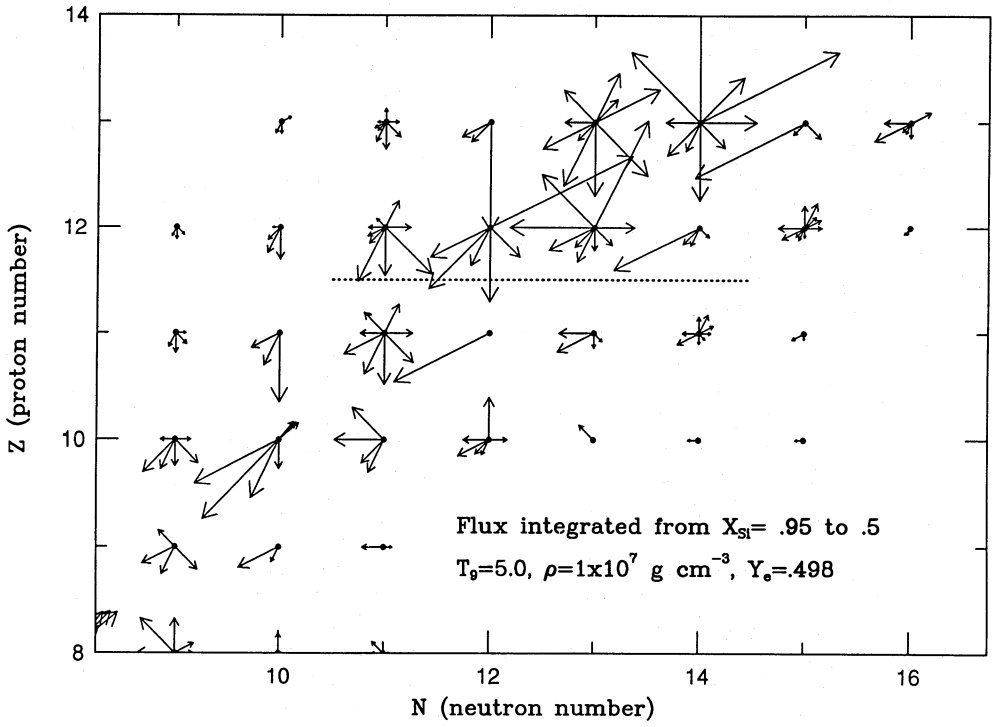

FIG. 5*a*

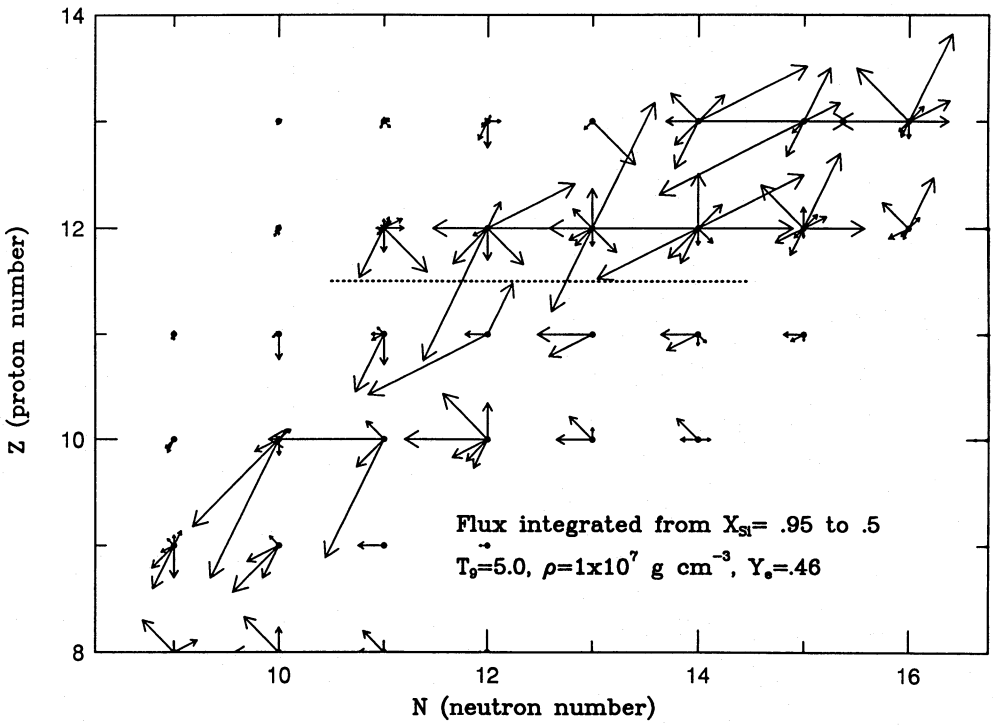

FIG. 5*b*

FIG. 5.—(*a*) Vector field representing the integrated reaction fluxes from X(Si group) = 0.95 to X(Si group) = 0.5, along the lower boundary of the silicon group, for $T_9 = 5.0$, $\rho = 10^7$ g cm^{-3}, and $Y_e = 0.498$. (*b*) Vector field representing the integrated reaction fluxes from X(Si group) = 0.95 to X(Si group) = 0.5, along the lower boundary of the silicon group, for $T_9 = 5.0$, $\rho = 10^7$ g cm^{-3}, and $Y_e = 0.46$. (*c*) Vector field representing the integrated reaction fluxes from X(Si group) = 0.95 to X(Si group) = 0.5, along the lower boundary of the silicon group, for $T_9 = 3.5$, $\rho = 10^9$ g cm^{-3}, and $Y_e = 0.498$. (*d*) Vector field representing the integrated reaction fluxes from X(Si group) = 0.1 to X(Si group) = 0.02, along the lower boundary of the silicon group, for $T_9 = 5.0$, $\rho = 10^7$ g cm^{-3}, and $Y_e = 0.498$. All vector magnitudes have logarithmic dependences on the size of the associated integrated fluxes.

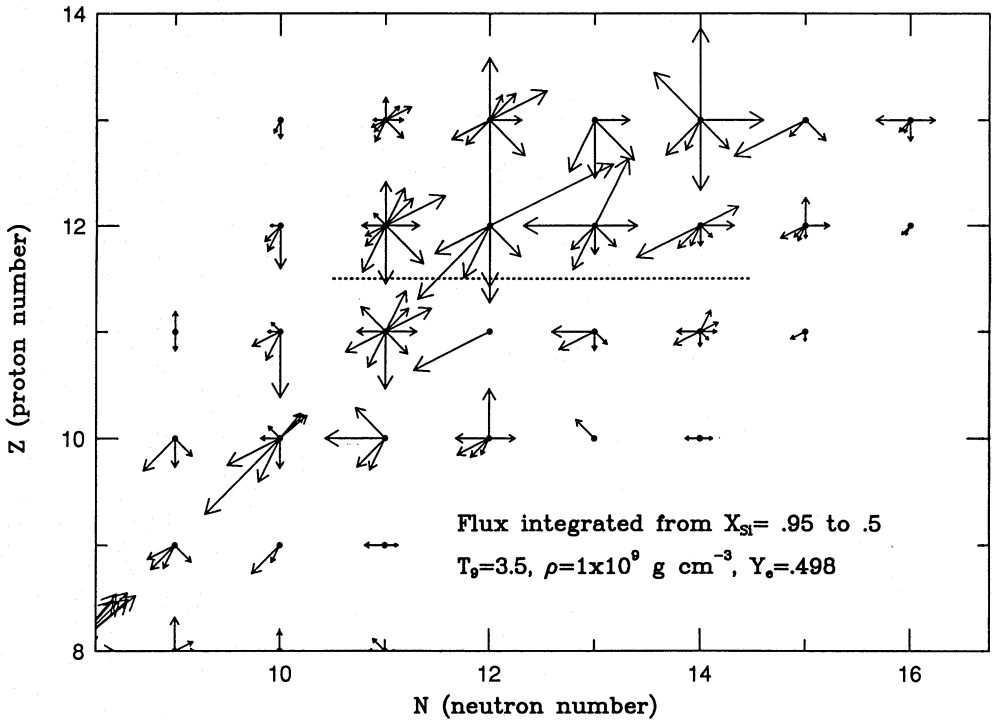

FIG. 5c

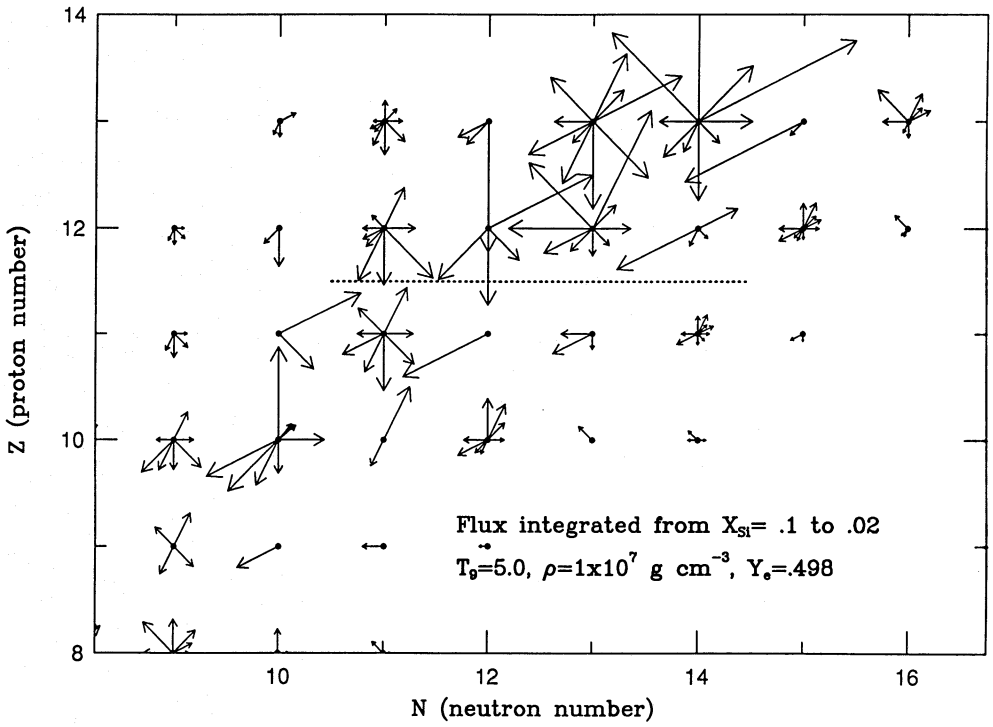

FIG. 5d

that at early times there are two definite QSE groups separated by a thin boundary region (see Fig. 1*c*). Although there are some relative changes in the abundances of these nuclei, variations of temperature, density, and degree of silicon exhaustion do not sharply alter the membership of this boundary region. In Figure 6*a* this boundary region is enclosed by the dotted line, with the lower edge of the iron peak group to the right and above, and the upper edge of the silicon group to the left and below. As revealed in Table 2, for $T_9 = 5.0$, $\rho = 10^7$ g cm^{-3}, and $Y_e = 0.498$, by X(Si group) = 0.5 there is a single well-established QSE group. In fact, for these conditions, the species which comprise the iron peak group have abundances within 10% of their silicon QSE abundances by the time X(Si group) $\sim$ 0.85. As a result, the vectors in Figure 6*a* represent the integrated reaction fluxes from X(Si group) = 0.95, by which time the two QSE groups are well established, until X(Si group) = 0.85. Thus these are the fluxes which bring the

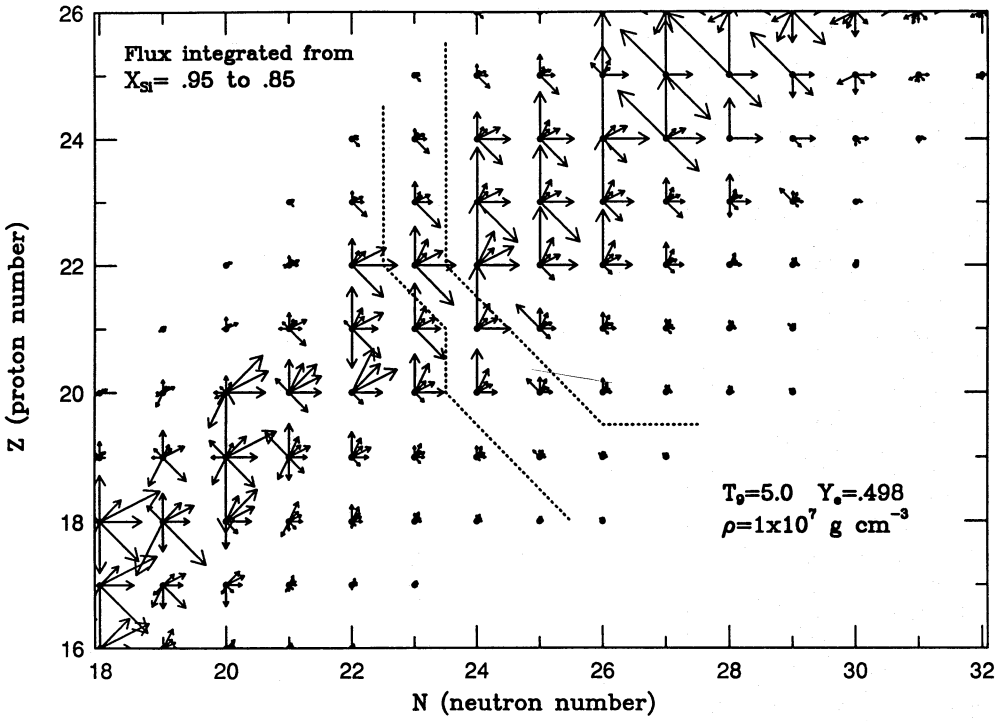

FIG. 6*a*

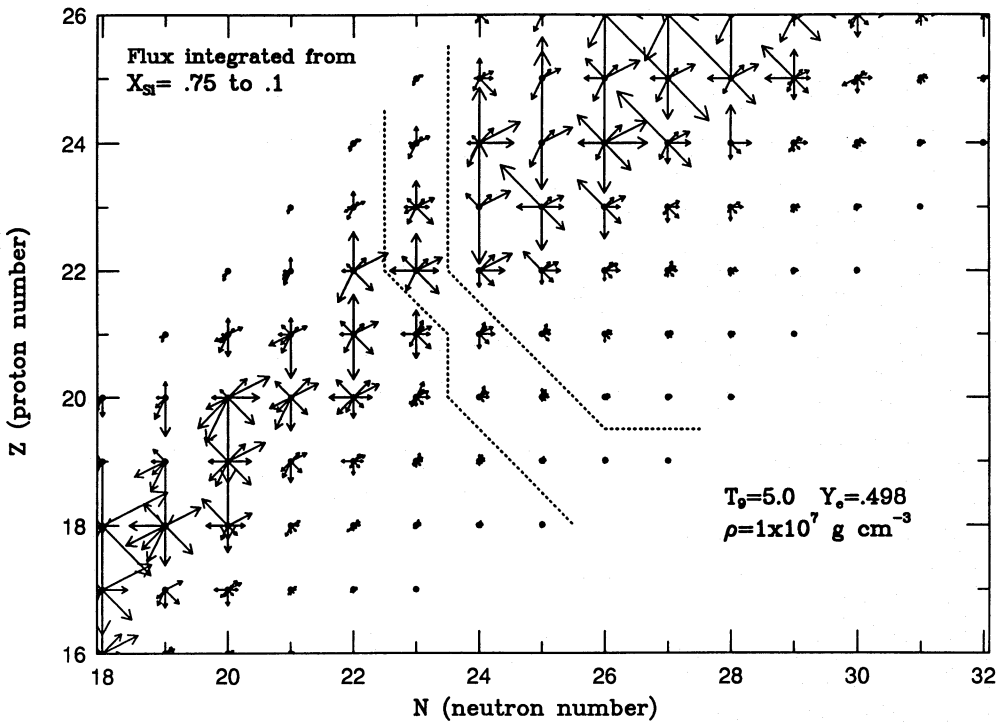

FIG. 6*b*

FIG. 6.—(*a*) Vector field representing the integrated reaction fluxes from X(Si group) = 0.95 to X(Si group) = 0.85, along the boundary between the silicon group and the iron peak group, for $T_9 = 5.0$, $\rho = 10^7$ g cm^{-3}, and $Y_e = 0.498$. (*b*) Vector field representing the integrated reaction fluxes from X(Si group) = 0.75 to X(Si group) = 0.1, along the boundary between the silicon group and the iron peak group, for $T_9 = 5.0$, $\rho = 10^7$ g cm^{-3}, and $Y_e = 0.498$. (*c*) Vector field representing the integrated reaction fluxes from X(Si group) = 0.95 to X(Si group) = 0.85, along the boundary between the silicon group and the iron peak group, for $T_9 = 3.5$, $\rho = 10^9$ g cm^{-3}, and $Y_e = 0.498$. (*d*) Vector field representing the integrated reaction fluxes from X(Si group) = 0.95 to X(Si group) = 0.5, along the boundary between the silicon group and the iron peak group, for $T_9 = 5.0$, $\rho = 10^7$ g cm^{-3}, and $Y_e = 0.46$. (*e*) Vector field representing the integrated reaction fluxes from X(Si group) = 0.5 to X(Si group) = 0.1, along the boundary between the silicon group and the iron peak group, for $T_9 = 5.0$, $\rho = 10^7$ g cm^{-3}, and $Y_e = 0.46$. All vector magnitudes have logarithmic dependences on the size of the associated integrated fluxes.

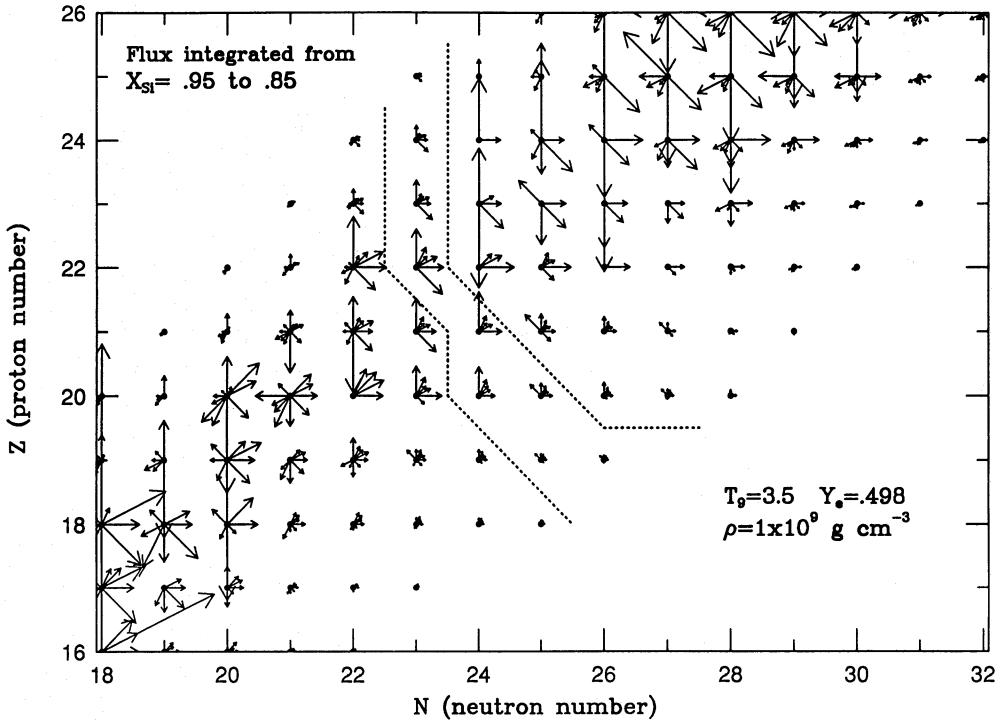

FIG. 6c

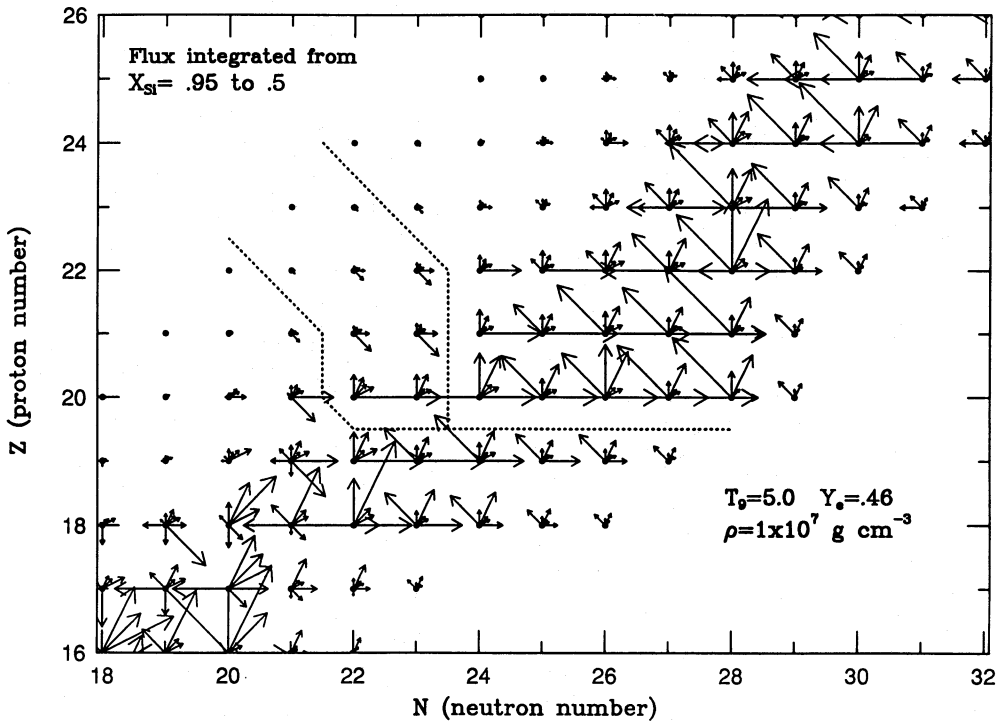

FIG. 6d

groups into QSE. It is therefore not surprising that there are no significant fluxes downward from the iron peak group into the boundary region, and similarly no fluxes into the silicon group which originate above. The dominant flux into the iron peak group is ^{45}Sc(p, γ)^{46}Ti. A number of other fluxes contribute, including ^{45}Ti(n, γ)^{46}Ti, ^{42}Ca(α, γ)^{46}Ti, ^{43}Sc(α, p)^{46}Ti, ^{46}V(n, p)^{46}Ti, and ^{44}Ti(α, p)^{47}V with fluxes relative to ^{45}Sc(p, γ)^{46}Ti of 0.12, 0.09, 0.04, 0.05, and 0.08, respectively. Thus ^{45}Sc(p, γ)^{46}Ti accounts for approximately 70% of the entire flux into the iron peak group. This agrees well with the findings of WAC for explosive burning at comparable densities. This agreement occurs in spite of differences over group membership between this work and WAC. In particular, WAC place ^{46}Sc as a member of the silicon group (those authors do not include a boundary region), while our results place it within the iron peak group for comparable Y_e. The existence of the boundary region causes a further complication, in that there is not a one-to-

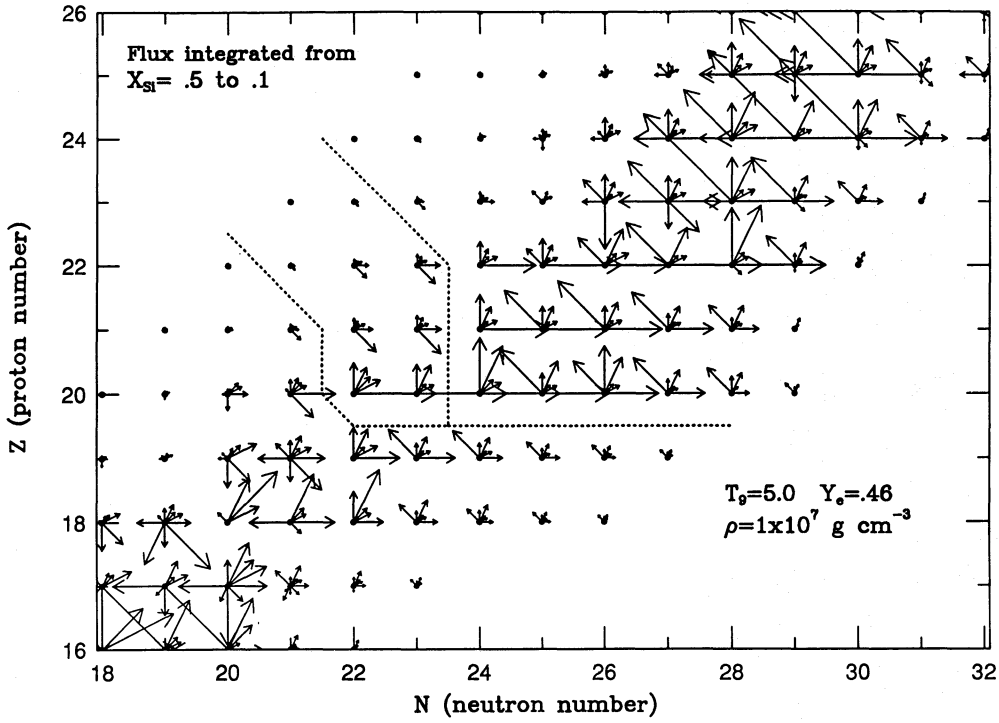

FIG. 6*e*

one correspondence between the flows out of the silicon group and those into the iron peak group. In addition to reactions like ^{44}Ti(α, p)^{47}V, ^{43}Sc(α, p)^{46}Ti, and ^{42}Ca(α, γ)^{46}Ti, which directly connect the silicon group to the iron peak group, there are a number of reactions which transfer mass from the silicon group into the boundary region. Principal among these are ^{42}Ca(α, n)^{45}Ti, ^{42}Ca(α, p)^{45}Sc, ^{44}Ti(n, γ)^{45}Ti, ^{44}Sc(p, γ)^{45}Ti, and ^{44}Sc(n, p)^{44}Ca, with fluxes relative to ^{45}Sc(p, γ)^{46}Ti of 0.28, 0.35, 0.21, 0.20, and 0.12, respectively. With this many reactions contributing significantly to the flow of mass into the boundary region, the dominance of ^{45}Sc(p, γ)^{46}Ti as a flow out of the boundary requires substantive reactions among the nuclei of the boundary region. Thus the relative values of $r_{QSE}(^AZ)$ revealed in Figure 1*c* for the nuclei within the boundary are representative of reaction flows within the region and not just a coincidental occurrence. Note in particular in Figure 1*c* that both ^{45}Ti and ^{44}Ca are relatively overabundant when compared to ^{45}Sc and that Figure 6*a* shows significant flow along ^{45}Ti(n, p)^{45}Sc and ^{44}Ca(p, γ)^{45}Sc. Thus the links within the boundary regions are important to the behavior of the boundary. The thin fringe of nuclei shown in Figure 1*c* between the silicon and the iron peak groups are not separate beads on strings of reactions between the QSE groups, but are part of an interconnected region which mediates the transfer of mass between the silicon and iron peak groups.

Once these two QSE groups are replaced by a single group, knowledge of the flows between the formerly separate groups is no longer essential, as these flows represent the changes required under QSE as the free-nucleon abundances converge toward equilibrium. In the case of $T_9 = 5.0$, $\rho = 10^7$ g cm^{-3}, and $Y_e = 0.498$, this means that the fluxes for X(Si group) < 0.8 reflect the movement of the mass into more proton-rich nuclei, as we discussed in § 5. Figure 6*b* shows the integrated fluxes from X(Si group) = 0.75 to X(Si group) = 0.1. The dominant fluxes between the former silicon and iron peak groups are a set of (α, p) reactions, principally ^{44}Ti(α, p)^{47}V, ^{43}Sc(α, p)^{46}Ti, and ^{45}Ti(α, p)^{48}V. Thus the dominant mass fluxes at late time proceed upward through more proton-rich nuclei than they did prior to the merger of the QSE groups. Another reflection of this tendency toward proton-rich nuclei is the domination of (n, p) reactions by (p, n) after group merger. Comparison of Figures 6*a* and 6*b* reveals that, while at early time there was considerable flux within the iron peak QSE group through reactions like ^{48}Cr(n, p)^{48}V and ^{47}V(n, p)^{47}Ti, after merger it is the reverse reactions, ^{48}V(p, n)^{48}Cr and ^{47}Ti(p, n)^{47}V in this case, which dominate. In another important reversal, at late times there are downward flows from the former iron peak group, most importantly ^{46}Ti(γ, p)^{45}Sc. For $T_9 = 3.5$, $\rho = 10^{10}$ g cm^{-3}, and $Y_e = 0.498$, a considerably greater density than any considered by WAC, the scenario is little changed. As is shown in Figure 6*c*, the dominant fluxes, during the time that two separate QSE groups persist, are still ^{45}Sc(p, γ)^{46}Ti, ^{45}Ti(n, γ)^{46}Ti, ^{42}Ca(α, γ)^{46}Ti, ^{43}Sc(α, p)^{46}Ti, ^{46}V(p, n)^{46}Ti, and ^{44}Ti(α, p)^{47}V, with relative fluxes of 1, 0.05, 0.23, 0.007, 0.007, and 0.32, respectively. Clearly there is much change in the relative fluxes, with ^{45}Sc(p, γ)^{46}Ti carrying only 60% of the flux into the iron peak group, but the change is merely in degree. The variation of temperature and density does not profoundly change which reaction fluxes bridge the gap between the iron peaks and silicon groups, though the relative importance can vary. Thus, for $Y_e = 0.498$ our analysis of the dominant reaction flows which transfer mass into the iron peak group is in excellent agreement with that of WAC. The dominance of ^{45}Sc(p, γ)^{46}Ti as the primary conduit of mass transfer into the iron peak group is readily apparent. At late times the (α, p) reactions on more proton-rich nuclei dominate, especially ^{44}Ti(α, p)^{47}V, while there is a downward flow via ^{46}Ti(γ, p)^{45}Sc. Both of these points support the earlier analysis of WAC.

We noted earlier that the variation of Y_e causes the mem-

bership of the QSE groups to change. These changes are reflected in the comparison of Figures 1*c* and 1*e*. As we discussed in § 4, the boundary region for smaller Y_e is displaced and noticeably broader in N. This new boundary region is enclosed within the dotted lines of Figure 6*d*, which shows the integrated fluxes for $T_9 = 5.0$, $\rho = 10^7$ g cm^{-3}, and $Y_e = 0.46$, from X(Si group) = 0.95 to X(Si group) = 0.5. Under these conditions the silicon and iron peak groups reach $\pm 5\%$ of merger for X(Si group) ~ 0.1. There is some ambiguity as to the group membership of the neutron-rich isotopes of K (^{43}K, ^{44}K, ^{45}K, and ^{46}K), as they seem to be members of the silicon group for X(Si group) ~ 0.9 with abundances approximately 60% of their silicon QSE abundance, while the members of the iron peak group are more than an order of magnitude underabundant (Fig. 1*e*). For X(Si group) ~ 0.5 (Fig. 1*f*), these K isotopes are still only approximately 80% of their silicon QSE abundance, while the iron peak group has converged to within a factor of 2. Examination of Figure 6*d* reveals that the reaction fluxes from these K isotopes into the neutron-rich isotopes of Ca are much smaller than the corresponding fluxes from Ca into Sc and are also much smaller than the flows into the boundary region from less neutron-rich isotopes of K and Ar. Thus their inclusion within the silicon group seems reliable though imperfect. The dominant fluxes out of the silicon group are ^{38}Ar(α, γ)^{42}Ca, ^{39}Ar(α, n)^{42}Ca, ^{40}Ar(α, n)^{43}Ca, ^{42}K(p, n)^{42}Ca, and ^{43}K(p, n)^{43}Ca, with relative fluxes of 0.47, 0.34, 1, 0.1, and 0.30, respectively. There is also a small group of reactions, most importantly ^{41}Ar(α, n)^{44}Ca, ^{42}Ar(α, n)^{45}Ca, ^{43}K(α, n)^{46}Sc, ^{44}K(p, n)^{44}Ca, and ^{45}K(p, n)^{45}Ca, which directly link the silicon group to the iron peak group. However, the sum of these fluxes is less than 15% of the flux carried by ^{40}Ar(α, n)^{43}Ca. These small fluxes are also only a minor contribution to the flux into the iron peak group, which is overwhelmingly dominated by ^{43}Ca(n, γ)^{44}Ca. The flux through this reaction is 2.3 times larger than the flux through ^{40}Ar(α, n)^{43}Ca and thus represents over 90% of the flux into the iron peak group. The flow within the iron peak group is dominated by a series of (n, γ) reactions between isotopes of Ca, out to ^{48}Ca. The flow upward from Ca is largely by (p, n) and (α, n) reactions. This transfer of mass into the iron peak nuclei via the neutron-rich isotopes of Ca is reminiscent of the exploratory results TA found for lower mass stars. In Figure 6*c* we examined the integrated fluxes for low temperature and high density, conditions one expects for core silicon burning in lower mass stars, but with $Y_e = 0.498$, and found little difference between the low-temperature/high-density case and the high-temperature/low-density case, except for an increase in the relative importance of flows through the more proton-rich nuclei. From Figure 6*d* we conclude that the flows through neutron-rich Ca which TA described are due to the greater neutronization found in the core of less massive stars.

Examination of Figure 6*e* reveals that the trend noted earlier for less neutron-rich nuclei to increase in importance at later times is also true for $Y_e = 0.46$. With merger of the QSE groups occurring for X(Si group) ~ 0.1 under these conditions, the integrated flux from X(Si group) = 0.5 to X(Si group) = 0.1 is still reflective of the flows which bring the groups to equilibrium. At these later times, the reaction ^{38}Ar(α, γ)^{42}Ca carries a larger flux than the reactions ^{39}Ar(α, n)^{42}Ca and ^{40}Ar(α, n)^{43}Ca combined. Although the dominant flow into the iron peak group is still ^{43}Ca(n, γ)^{44}Ca, comparison of Figure 6*e* to Figure 6*d* shows that the series of large fluxes through (n, γ) reactions on Ca isotopes is greatly diminished for ^{46}Ca and ^{47}Ca. Instead the flow proceeds upward at lower N. This process continues after group merger as the average Z/A within the iron peak group approaches Y_e. Clearly the convergence of the average Z/A within the iron group toward Y_e, as we discussed in § 5, plays a role in making proton-rich nuclei more important as silicon is exhausted. With the iron group dominated at early times by nuclei with $Z/A < Y_e$, the reactions through the neutron-rich isotopes are naturally enhanced by the increased abundance. As the abundance of free neutrons declines from the initial overabundance, the relative importance of the less neutron-rich nuclei, reflected by the average Z/A, grows. This is particularly true at low Y_e, since the silicon group is dominated by nuclei with $Z/A \sim 0.5$.

Thus the reactions which bridge the gap between the silicon group and the iron peak group reflect the underlying changes in abundance. The interconnection of these groups is also reflective of the group membership and of changes in the relative importance of these members. For high Y_e the dominant flow into the iron peak group prior to the merger of the groups is ^{45}Sc(p, γ)^{46}Ti. The flow which feeds ^{45}Sc exits the silicon group via a series of reactions involving ^{40}Ca, ^{42}Ca, ^{43}Sc, ^{44}Sc, ^{44}Ti, and ^{45}Ti. For somewhat smaller Y_e the flow into the iron peak group via ^{45}Sc(p, γ)^{46}Ti is still important, but it is now fed through reactions involving ^{42}Ca, ^{44}Ca, and ^{46}Sc. As the degree of neutronization increases, the dominant flow between the groups naturally winds its way through more neutron-rich nuclei as the abundances of these nuclei become more important. For $Y_e = 0.46$ this means that the merger is achieved via a flow that proceeds through a long series of (n, γ) captures on Ca. As time proceeds, as we showed in § 5, the average Z/A within the iron peak group converges toward the global value of Y_e. The network of reactions responds to (or causes) this greater abundance of less neutron-rich nuclei by increasing the importance of bridging reactions involving more proton-rich nuclei and by increasing the flux through (p, n) reactions within the iron peak group. It is the neutronization of material which dominates the behavior of the QSE groups, and therefore the reactions that merge the groups. Although the variation of Y_e has little effect on the cross sections and rate coefficients, the reaction flows across the boundary change in response to the changing abundances within the groups. Since these reactions, particularly those from the bottom of the silicon QSE group, govern the rate of conversion of silicon into iron peak nuclei, these differences in reaction flows will clearly be reflected in the rate of energy production.

7. ENERGETICS OF SILICON BURNING

Before we examine the energy production from the actual network calculations, it is instructive to make some simple energetic arguments about silicon burning. If we take as the final distribution of each of our constant temperature, density, and Y_e cases the corresponding screened NSE distribution and compare this with the initial distribution, we can calculate the amount of energy available from silicon burning. Table 4 shows the binding energies of the initial and NSE distributions and their difference for a few cases, all in ergs per gram. Comparison of cases which differ only in Y_e reveals that much more energy is available at lower Y_e. This reflects the larger binding energy per nucleon of ^{56}Fe, ^{54}Fe, and ^{58}Ni in comparison to ^{56}Ni, a fact which, for

TABLE 4

ENERGY RESERVOIR

T_9	ρ (cm^{-3})	Y_e	Initial BE[a] (ergs g^{-1})	NSE BE (ergs g^{-1})	Difference (ergs g^{-1})
3.5.....	10^7	0.498	8.155×10^{18}	8.346×10^{18}	1.91×10^{17}
		0.48	8.193×10^{18}	8.431×10^{18}	2.38×10^{17}
		0.46	8.172×10^{18}	8.477×10^{18}	3.05×10^{17}
3.5.....	10^{10}	0.498	8.155×10^{18}	8.348×10^{18}	1.93×10^{17}
		0.49	8.172×10^{18}	8.386×10^{18}	2.14×10^{17}
		0.48	8.193×10^{18}	8.431×10^{18}	2.38×10^{17}
		0.47	8.214×10^{18}	8.461×10^{18}	2.47×10^{17}
		0.46	8.172×10^{18}	8.479×10^{18}	3.07×10^{17}
5.0.....	10^7	0.498	8.155×10^{18}	8.198×10^{18}	0.43×10^{17}
		0.49	8.172×10^{18}	8.283×10^{18}	1.11×10^{17}
		0.48	8.193×10^{18}	8.369×10^{18}	1.76×10^{17}
		0.47	8.214×10^{18}	8.420×10^{18}	2.06×10^{17}
		0.46	8.172×10^{18}	8.452×10^{18}	2.80×10^{17}
5.0.....	10^{10}	0.498	8.155×10^{18}	8.345×10^{18}	1.90×10^{17}
		0.48	8.193×10^{18}	8.424×10^{18}	2.31×10^{17}
		0.46	8.172×10^{18}	8.472×10^{18}	3.00×10^{17}

[a] Binding energy.

example, accounts for much of the light curve of supernovae. The comparison of cases which differ in temperature and density shows a greater availability of energy at lower temperatures and higher densities. The lower the temperature, the more the exp $[B(^4Z)/kT]$ term in the nuclear Saha equation dominates, causing a more prominent peak in the abundance distribution composed of the most bound nuclei. Similarly, a higher density also favors more massive nuclei which (up to Ni/Fe) have a larger binding energy. For example, for $Y_e = 0.498$ and $\rho = 10^{10}$ g cm^{-3}, the change from $T_9 = 3.5$ to $T_9 = 5.0$ causes a change in the mass fraction concentrated in isotopes of Mn, Fe, Co, and Ni, from 0.9996 to 0.996. For $Y_e = 0.498$ and $\rho = 10^7$ g cm^{-3}, the same change in temperature results in changes in this mass fraction from 0.9991 to 0.918. With as much as 6 times more energy available per silicon nucleus at low Y_e, even if the rate of silicon depletion is the same in all cases, there can be tremendous differences in the energy generation and therefore in the hydrodynamic conditions which cause this process. This is particularly important as electron captures cause Y_e to drop.

The lack of a single dominating reaction in silicon burning makes prediction of the energy production complicated. In general, the rate of energy production per gram by a nuclear process, ϵ, is given in terms of the reaction rates, r_{ij} (reactions cm^{-3} s^{-1}), by

$$\epsilon = \frac{1}{\rho} \sum_{ij} r_{ij} Q_{ij} , \tag{15}$$

where Q_{ij} is the Q-value for the reaction between i and j. In cases where a single reaction dominates the process the sum is unnecessary. Although it is possible, as was shown above, to calculate the energy store available for silicon burning, the plethora of possible governing reactions revealed in § 6 makes estimation of the temporal behavior of this energy release difficult. For each reaction ij in silicon burning, there is a reverse reaction kl which is approaching equilibrium with it. Thus equation (15) becomes

$$\epsilon = \frac{1}{\rho} \sum_{ij} (r_{ij} - r_{kl(ij)}) Q_{ij} , \tag{16}$$

where $Q_{kl} = -Q_{ij}$. As the abundances approach equilibrium, ϵ approaches zero, not necessarily because of the exhaustion of fuel but because each pair of reactions is balancing. While Table 4 shows the global value of $E = \int_0^{\rm NSE} \epsilon \, dt$, it says nothing about the interplay of the various r_{ij} and r_{kl}. These, however, determine the temporal behavior of ϵ.

In § 6 we concluded that there are significant differences in the relative importance of the many reaction flows which typify silicon burning. In particular, the variation of Y_e has a profound effect on which reactions are the most important links between the QSE groups and which reactions are primarily responsible for flow downward from the silicon group. Examination of Figure 7*a* shows that these differences in reactions result in tremendous variation in ϵ as a function of X(Si group) and Y_e. These particular curves are for $T_9 = 5$ and $\rho = 10^7$ g cm^{-3}. While the behavior is similar in each case as equilibrium is approached, the initial stages, which are the most important from the point of view of energy production, vary greatly. Clearly the different reactions which dominate as Y_e varies result in very different behavior. As we noted in § 4, the lower Y_e cases take less time to reach a similar degree of silicon exhaustion. Table 5 shows the elapsed time for several degrees of silicon exhaustion. Silicon burning at $Y_e = 0.498$ is much slower than silicon burning at $Y_e = 0.46$. With the elapsed time to X(Si group) ~ 0.9 almost an order of magnitude larger for high Y_e and the energy available, the global E, much smaller, it is not surprising that ϵ for $Y_e = 0.498$ is more than an order of magnitude smaller than ϵ for $Y_e = 0.46$ at early times. Further, with the elapsed time between X(Si group) ~ 0.5 and 0.1 being more than 100 times larger for $Y_e = 0.498$ than for $Y_e = 0.46$, it is not surprising that ϵ falls off more precipitously for higher Y_e. These very different temporal evolutions in energy generation are then directly attributable to the very different fluxes seen in § 6. Clearly simple approximations which multiply a temperature- and density-dependent formula for ϵ by a correction dependent on Y_e are ruled out. The behavior with changing Y_e is dependent on the complex interaction of the different reactions out of the silicon group. Figure 7*b* shows that at high density/low temperature there is a similar tangle of curves as a function

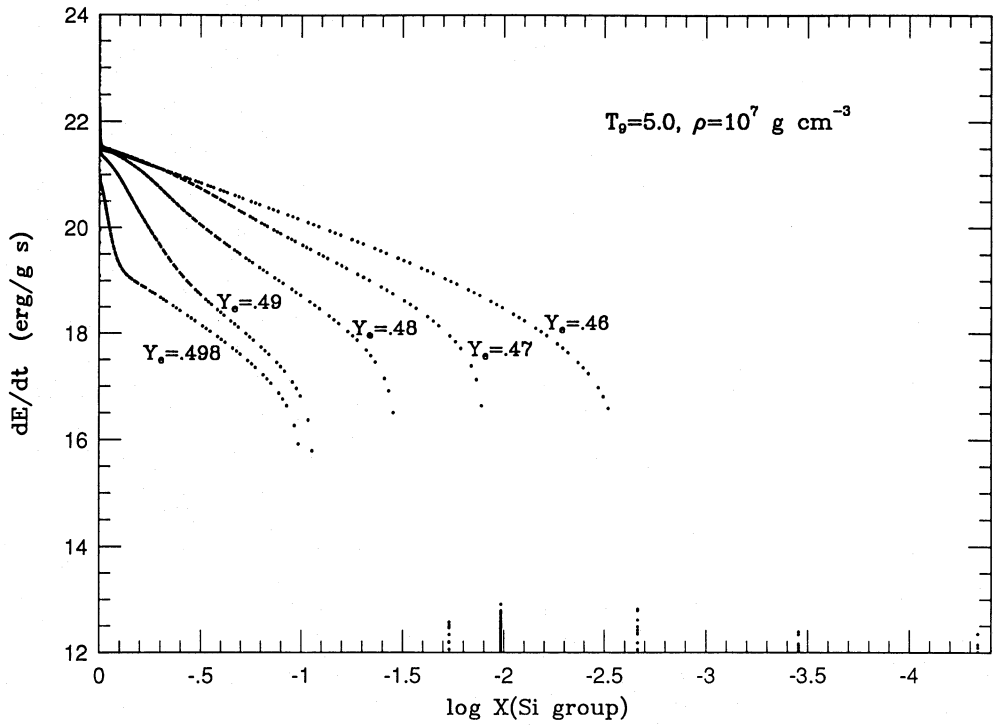

FIG. 7a

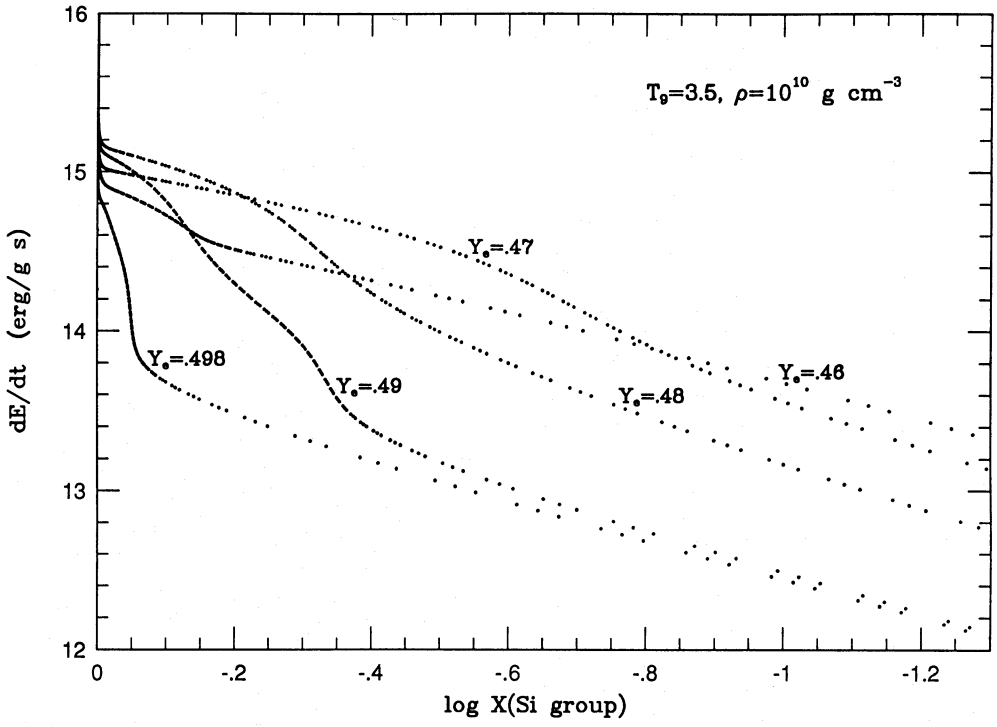

FIG. 7b

FIG. 7.—(*a*) Rate of energy generation as a function of degree of silicon exhaustion, for $T_9 = 5.0$, and $\rho = 10^7$ g cm^{-3}, with Y_e varying from 0.498 to 0.46. (*b*) Rate of energy generation as a function of degree of silicon exhaustion, for $T_9 = 3.5$, and $\rho = 10^{10}$ g cm^{-3}, with Y_e varying from 0.498 to 0.46.

of Y_e. Any successful approximation of the energy generation for silicon burning needs to take into account the complex behavior of the reactions out of the QSE groups. As we established in §§ 4 and 5, the reactions within the groups can be well understood by the use of QSE. The many reactions, shown in § 6 to be important for the understanding of the flows among the groups, are also the governing reactions here, particularly those reactions which transfer mass downward from the silicon group. The sheer number of important reactions, and their response to changes in Y_e and degree of silicon exhaustion, preclude a simple analytic model. Instead, in Paper II, we will discuss a promising approximation to the network calculation of silicon burning employing QSE. For now, however, we will

TABLE 5

ELAPSED TIME VERSUS DEGREE OF SILICON EXHAUSTION

CONDITIONS			ELAPSED TIME (S)		
T_9	ρ (g cm^{-3})	Y_e	X(Si group) = 0.9	X(Si group) = 0.5	X(Si group) = 0.1
5.0	10^7	0.498	5.6×10^{-5}	1.9×10^{-3}	3.6×10^{-2}
5.0	10^7	0.48	8.0×10^{-6}	7.2×10^{-5}	1.7×10^{-3}
5.0	10^7	0.46	1.1×10^{-5}	5.8×10^{-5}	2.6×10^{-4}
5.0	5×10^7	0.46	1.1×10^{-5}	5.8×10^{-5}	2.5×10^{-4}
5.0	2×10^8	0.46	1.0×10^{-5}	5.5×10^{-5}	2.2×10^{-4}
5.0	10^9	0.46	9.4×10^{-6}	5.0×10^{-5}	2.0×10^{-4}
5.0	10^{10}	0.46	7.9×10^{-6}	4.1×10^{-5}	1.5×10^{-4}
4.5	10^{10}	0.46	4.7×10^{-4}	2.6×10^{-3}	8.8×10^{-3}
4.0	10^{10}	0.46	6.6×10^{-2}	4.4×10^{-1}	1.6×10^{0}
3.5	10^{10}	0.46	3.3×10^{1}	2.8×10^{2}	1.1×10^{3}

discuss a few additional general characteristics of the energy generation during silicon burning.

One particularly noteworthy feature, common to all of the cases pictured in Figure 7*a*, is the tail-off, with the energy generation actually becoming an energy depletion before the silicon group reaches its equilibrium value. This occurs once the iron peak nuclei dominate the mass fraction and thus the energy generation from the destruction of silicon group elements has dropped. The convergence of the free-proton and free-neutron fractions to their equilibrium values results in an increasing portion of the mass within the iron peak group found in elements with higher Z and A. These nuclei are not as bound as the Fe and Ni isotopes which dominate the NSE distribution, hence their production is endoergic. Furthermore, the production of the free nucleons is also endoergic. As Y_e decreases, the equilibrium mass fraction of these nuclei increases, requiring more energy to produce them and therefore causing the tail-off to begin further from equilibrium, i.e., while the energy generated from the conversion of silicon into iron peak nuclei is larger. This results in the increasing gap between the last positive value of the energy generation and the equilibrium silicon group mass fraction as Y_e decreases. For $Y_e \sim 0.5$, this effect is exacerbated by the transition as silicon exhaustion increases in which nucleus is most abundant. It is this transition, demonstrated in Figure 3*a*, from ^{56}Fe and ^{54}Fe to the less bound ^{56}Ni which is responsible for the sharp decline of ϵ seen for larger values of Y_e.

Figure 8*a* shows the effect of temperature variations on ϵ, for $\rho = 10^{10}$ g cm^{-3} and $Y_e = 0.46$. The resemblance these curves share is striking. Each is a power law which tails off as each case approaches equilibrium. The lack of convergence between these curves indicates that changes due to variations in temperature are variations in rates, not changes in the relative importance of different reactions, which agrees with our analysis of the reaction fluxes in § 6. From Table 4 it is apparent that the available energy supply is essentially unchanged by temperature variations for this density. Thus the differences in ϵ are due to differing timescales for the burning. Comparison of the times necessary for these conditions to result in 10% exhaustion of the silicon group attest to this assertion. From the elapsed times for X(Si group) ~ 0.9 shown in Table 5, we find that the differences in ϵ are very similar to the differences in elapsed time. Clearly the increase in temperature increases the photodissociation rates, thus providing for quicker destruction of the silicon group. However, the variation in timescale with temperature is not consistent with the variations in the photodisintegration rate of ^{28}Si. This is in keeping with the argument by BCF, supported by our analysis, that it is not the photodissociation rate of silicon which governs the rate of silicon destruction; rather, it is the downward flow from the silicon group which determines the burning timescale.

Variations in density have effects similar to those of temperature. Figure 8*b* portrays the effects of the variation of density, for $T_9 = 5.0$ and $Y_e = 0.46$. Once again we see the power laws that tail off as each case approaches its equilibrium. Note that the variation of ϵ with density, particularly at early times, is small. The variations in elapsed time to reach various degrees of silicon exhaustion as a function of density are also shown in Table 5. The ratio of ϵ for $\rho = 10^{10}$ g cm^{-3} to that for $\rho = 10^7$ g cm^{-3} is only 1.5 for X(Si group) ~ 0.9, and 1.4 for X(Si group) ~ 0.5. Within the silicon QSE group, the increase in density results in an increase in the relative importance of Mg. The ratio of the mass fractions in Mg for $\rho = 10^{10}$ g cm^{-3} compared to that for $\rho = 10^7$ g cm^{-3} is 1.3 both X(Si group) ~ 0.9 X(Si group) ~ 0.5. This suggests that the difference in the energy generation rate as a function of density is largely due to differences in QSE abundances and in the reaction flows which result from them.

In this section we showed that increases in temperature or density have large effects on the rate of energy generation, greatly enhancing the rate at which silicon is destroyed. Variations in neutronization also have a large effect on the rate of energy generation, changing the reaction pathways by which silicon is converted into iron peak elements. Thus, the evidence presented in this section points to the need to approximate the complete behavior of silicon burning in order to approximate the energy generation. This requires keeping track of many of the 300 nuclei and 3000 reactions used in this nuclear network. Fortunately, as we will show in a subsequent paper, QSE provides the means to approximate energy generation accurately at considerable savings in computation. QSE greatly reduces the number of reactions which need to be considered, since only those which leave their group are important to the evolution of the abundances within the group. Further, the prediction of abundances based on the QSE abundances greatly reduces the amount of nuclear accounting which must be done.

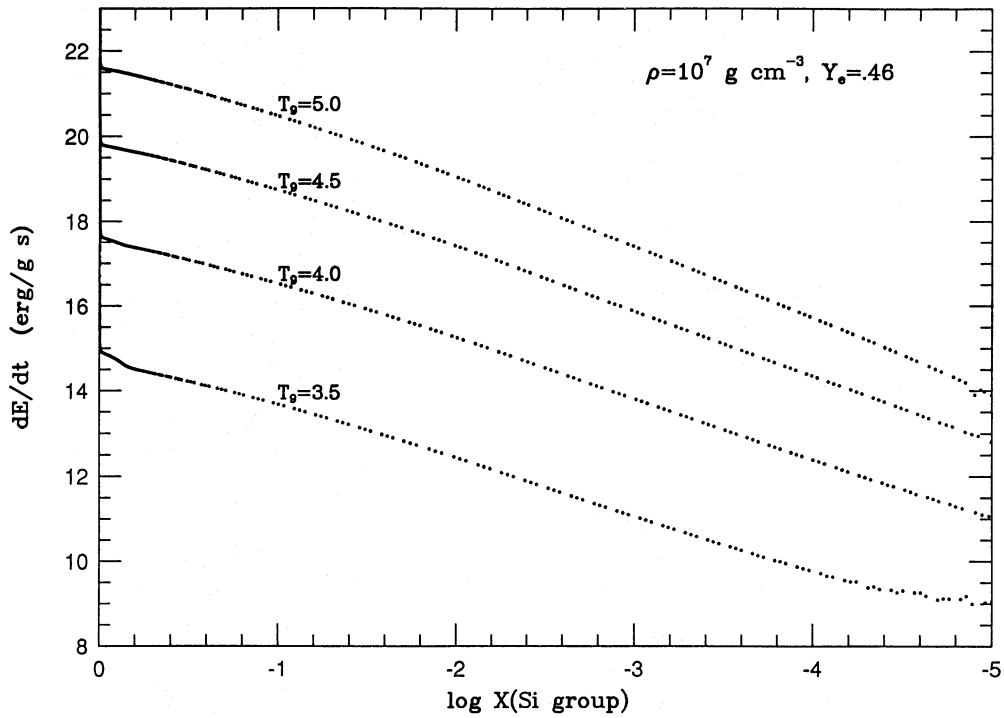

FIG. 8*a*

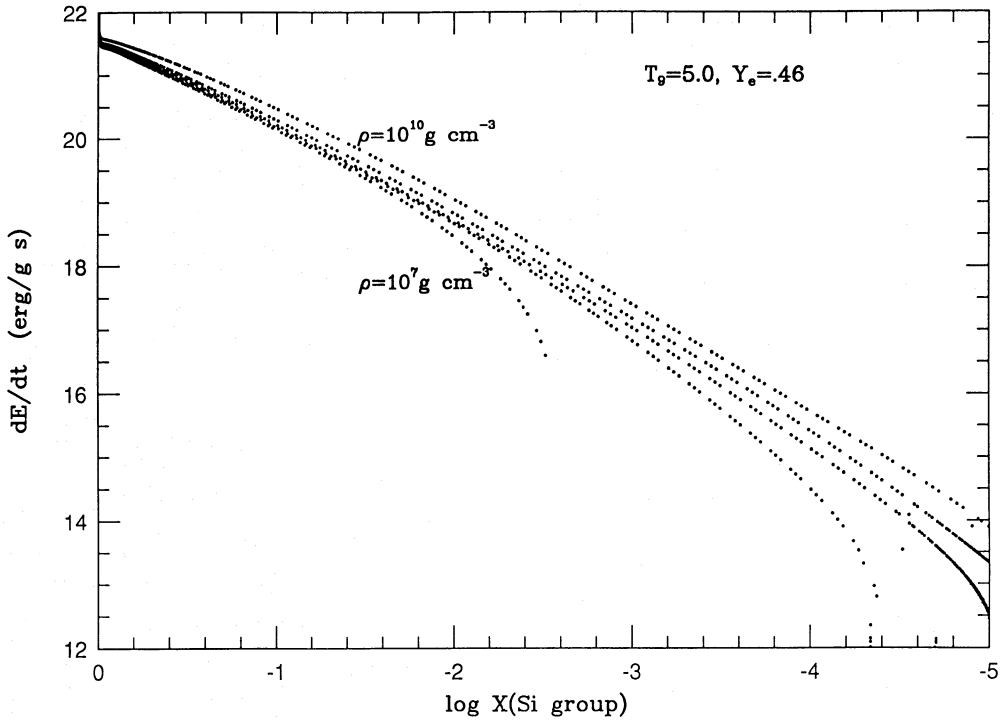

FIG. 8*b*

FIG. 8.—(*a*) Rate of energy generation as a function of degree of silicon exhaustion, for $\rho = 10^7$ g cm^{-3} and $Y_e = 0.46$, with T_9 varying from 3.5 to 5.0. (*b*) Rate of energy generation as a function of degree of silicon exhaustion, for $T_9 = 5.0$ and $Y_e = 0.46$, with ρ varying from 10^7 to 10^{10} g cm^{-3}.

8. CONCLUSIONS

We have performed a detailed reexamination of silicon burning as a function of temperature, density, and neutronization, using a large nuclear network. Central to understanding this process is the concept of quasi-equilibrium. A natural extension of nuclear statistical equilibrium, which it approaches in the asymptotic limit, quasi-equilibrium reflects the near-balance of the rapid formation and destruction of nuclei during silicon burning. The net gain in abundance of a species is much smaller than either its formation or its destruction rates. We rederived the equations of QSE, including for the first time the effects of Coulomb screening on the equilibrium distribution. This has been found by Hix

et al. (1996) to be important for NSE, and we showed that Coulomb screening is also important in reconciling the network abundance calculations with QSE. We further demonstrated the real usefulness of QSE in describing the network evolution, with many of the most abundant nuclei forming two QSE groups, one focused on silicon and the other on the iron peak nuclei. While previous authors have seen such separate groups at early times, we discovered that, with increasing neutronization, the separation of these groups persists through a much more significant portion of silicon burning. Furthermore, we showed not only that the duration of this two-group phase is a function of Y_e, but also that the membership in the groups is dependent on Y_e. Since previous work ignored extensive variation of neutronization and its effect on QSE, this behavior has not been seen before.

We demonstrated the effects of these interacting QSE groups on the abundances as the distribution evolves. One noticeable effect is the excessive production of neutron-rich iron peak nuclei during incomplete silicon burning, resulting in an iron peak group noticeably more neutronized than the global neutronization would imply. This effect is missed by many approximations to silicon burning, particularly those using narrow nuclear networks. With QSE governing the relative abundances within the groups, the principal evolution of the distribution is due to the reactions linking the groups. We further demonstrated that the important reactions for the destruction of silicon and the formation of iron peak nuclei are highly dependent on the degree of neutronization. While variations in temperature and density affect the relative rates of reactions and the overall speed of silicon destruction, they do not radically alter the reaction paths into and out of the QSE groups in the way that the variation of Y_e does. For relatively unneutronized material, the principal reaction flow linking the silicon group with the iron peak group proceeds through isotopes of Sc and Ti on the proton-rich side of stability, in agreement with WAC. For larger neutronization, the increasing availability of free neutrons, and the corresponding changes in QSE group membership, result in the dominant flow proceeding through neutron-rich isotopes of Ca, as TA suggested. Furthermore, the rate at which matter flows along these reaction paths is also strongly enhanced under these conditions. With the entire process and especially the rate of silicon destruction strongly dependent on Y_e, it is not surprising to find that the energy generation by silicon burning has a strong and complex dependence on Y_e. As we also showed, the variations in energy generation due to changes in temperature and density are not as convoluted as those due to changes in Y_e.

Taken together, these effects of neutronization on the process of silicon burning imply that successful modeling of silicon burning in its hydrodynamic context needs to account for the variety of reaction paths and full range of important nuclei. Because large networks like the one used here are a cumbersome addition to hydrodynamic calculations, much previous work has tried to approximate silicon burning using narrow networks and other simplified schemes. The present results warn of the danger of applying such schemes, developed for slight neutronization ($Y_e \sim 0.5$), beyond the context in which they were developed. In the context of reduced nuclear reaction networks, this implies that the networks not only need to stretch from H to the iron peak but also must have considerable breadth. This seemingly returns us to the cumbersome large networks. However, in a forthcoming paper we will demonstrate an alternative. Instead of reducing the number of nuclei by restricting the width, we find it possible to use the physics of QSE to intelligently reduce the number of abundances which must be evolved to a more manageable size.

The list of people who have contributed to this work is naturally larger than the author list. In particular, we would like to thank Dave Arnett, Ken Nomoto, and Masaki Hashimoto for motivating this work, and Al Cameron for his interest and aid. W. R. H. was supported in part by a NASA Graduate Student Researcher Fellowship. F.-K. T. was supported in part by NSF grant 89-13799 and the Swiss Nationalfonds.

REFERENCES

Aufderheide, M., Baron, E., & Thielemann, F.-K. 1991, ApJ, 370, 630
Bao, Z. Y., & Käppeler, F. 1987, At. Data Nucl. Data Tables, 36, 411
Bodansky, D., Clayton, D. D., & Fowler, W. A. 1968, ApJS, 16, 299 (BCF)
Burbidge, E. M., Burbidge, G. R., Fowler, A. A., & Hoyle, F. 1957, Rev. Mod. Phys., 29, 547 (B^2FH)
Caughlan, G. R., & Fowler, W. A. 1988, At. Data Nucl. Data Tables, 40, 283
Cowan, J. J., Thielemann, F.-K., & Truran, J. W. 1991, Phys. Rep., 208, 267
Fowler, W. A., & Hoyle, F. 1964, ApJS, 201
Graboske, H. C., De Witt, H. E., Grossman, A. S., & Cooper, M. S. 1973, ApJ, 181, 457
Hartmann, D., Woosley, S. E., & El Eid, M. F. 1985, ApJ, 297, 837
Hayashi, C., Nishida, M., Ohyama, N., & Tsuda, H. 1959, Prog. Theor. Phys., 22, 101
Hix, W. R., & Thielemann, F.-K. 1966, ApJ, submitted (Paper II)
Hix, W. R., Thielemann, F.-K., Fushiki, I., & Truran, J. W. 1996, ApJ, submitted
Itoh, N., Kuwashima, F., & Munakatu, H. 1990, ApJ, 362, 620
Michaud, G., & Fowler, W. A. 1972, ApJ, 173, 157
Nomoto, K., & Hashimoto, M. 1988, Phys. Rep., 163, 13
Thielemann, F.-K., & Arnett, W. D. 1985, ApJ, 295, 604 (TA)
Thielemann, F.-K., Arnould, M., & Truran, J. W. 1987, in Advances in Nuclear Astrophysics, ed. E. Vangioni-Flam, J. Audouze, M. Cassé, J.-P. Chièze, & J. Tran Thanh Van (Gif-sur-Yvette: Editions Frontières), 525
Thielemann, F.-K., Bitouzet, J.-P., Kratz, K.-L., Möller, P., Cowan, J. J., & Truran, J. W. 1993, Phys. Rep, 227, 269
Thielemann, F.-K., Hashimoto, M., & Nomoto, K. 1990, ApJ, 349, 222
Thielemann, F.-K., Nomoto, K., & Hashimoto, M. 1994, in Les Houches, Session LIV, Supernovae, ed. S. Bludman, R. Mochkovitch, & J. Zinn-Justin (Amsterdam: Elsevier), 629
Truran, J. W., Cameron, A. G. W., & Gilbert, A. 1965, Canadian J. Phys., 44, 563
Wagoner, R. V. 1969, ApJS, 18, 247
Wagoner, R. V., Fowler, W. A., & Hoyle, F. 1967, ApJ, 148, 3
Weaver, T. A., Woosley, S. E., & Fuller, G. M. 1985, in Numerical Astrophysics, ed. J. Centrella, J. Leblanc, & R. Bowers (Boston: Jones & Bartlett), 374
Wiescher, M., Görres, J., Graaf, S., Buchmann, L., & Thielemann, F.-K. 1989, ApJ, 343, 352
Wiescher, M., Görres, J., Thielemann, F.-K., & Ritter, H. 1986, A&A, 160, 56
Wiescher, M., Harms, V., Görres, J., Thielemann, F.-K., & Rybaryck, L. J. 1987, ApJ, 316, 162
Woosley, S. E. 1986, in 16th Advanced Course of the Swiss Society of Astrophysics and Astronomy, Nucleosynthesis and Chemical Evolution, ed. B. Hauck, A. Maeder, & G. Meynet (Geneva: Geneva Obs. Press), 1
Woosley, S. E., Arnett, W. D., & Clayton, D. D. 1973, ApJS, 26, 231 (WAC)
Woosley, S. E., & Hoffman, R. 1992, ApJ, 395, 202
Woosley, S. E., Pinto, P. A., & Weaver, T. A. 1988, Proc. Astron. Soc. Australia, 7, 355